Available online at www.sciencedirect.com
SCIENCE DIRECT®
Mechanics of Materials 37 (2005) 1007–1025
MECHANICS OF MATERIALS
www.elsevier.com/locate/mechmat

A continuum shape sensitivity method for fracture analysis of orthotropic functionally graded materials

B.N. Rao [a,*], Sharif Rahman [b]

[a] *Structural Engineering Division, Department of Civil Engineering, Indian Institute of Technology, Madras, Chennai 600 036, India*
[b] *Department of Mechanical Engineering, The University of Iowa, Iowa City, IA 52242, United States*

Received 10 February 2004; received in revised form 10 October 2004

Abstract

This paper presents a new continuum shape sensitivity method for calculating the mixed-mode stress-intensity factors of a stationary crack in two-dimensional, linear-elastic, orthotropic functionally graded materials with arbitrary geometry. The method involves the material derivative concept taken from continuum mechanics, the mutual potential energy release rate, and direct differentiation. Since the governing variational equation is differentiated prior to discretization, resulting sensitivity equations are independent of approximate numerical techniques, such as the finite element method, boundary element method, mesh-free method, or others. The discrete form of the mutual potential energy release rate is simple and easy to calculate, as it only requires multiplication of displacement vectors and stiffness sensitivity matrices. By judiciously selecting the velocity field, the method only requires displacement response in a subdomain close to the crack tip, thus making the method computationally efficient. Three finite-element based numerical examples, which comprise mode-I and mixed-mode deformations, are presented to evaluate the accuracy of the fracture parameters calculated by the proposed method. Comparisons have been made between stress-intensity factors predicted by the proposed method and available reference solutions in the literature, generated either analytically or numerically using various other fracture integrals or analyses. Excellent agreement is obtained between the results of the proposed method and previously obtained solutions. Therefore, shape sensitivity analysis provides an attractive alternative to fracture analysis of cracks in homogeneous and non-homogeneous orthotropic materials.

Keywords: Crack; Orthotropic functionally graded materials; Shape sensitivity analysis; Velocity field; Material derivative; Finite element method; Stress-intensity factor; Potential energy release rate

* Corresponding author. Tel.: +91 44 22578498; fax: +91 44 22578327.
E-mail address: bnrao@iitm.ac.in (B.N. Rao).

0167-6636/$ - see front matter © 2005 Elsevier Ltd. All rights reserved.
doi:10.1016/j.mechmat.2005.01.001

1. Introduction

Functionally graded materials (FGMs) that possess a nonuniform microstructure with continuously graded mechanical/thermal macro properties are essentially multi-phase particulate composites engineered to meet a predetermined functional performance such that the volume fraction of constituent materials vary smoothly (Suresh and Mortensen, 1998; Erdogan, 1995). Given the nature of processing techniques, graded materials can become anisotropic. For example, graded materials processed by a plasma spray technique generally have a lamellar structure (Sampath et al., 1995), whereas processing by electron beam physical vapor deposition would lead to a highly columnar structure (Kaysser and Ilschner, 1995). Such materials would not be isotropic, but orthotropic, with material directions that can be considered perpendicular to one another in an initial approximation. In recent years, various theoretical, computational, and experimental studies have been conducted to understand the fracture behavior of FGMs. A collection of technical papers, published in Volume 69, Issues 14–16 of (Paulino, 2002) *Engineering Fracture Mechanics* reflects such state-of-the-art research into FGM fracture. A major component of such studies involves calculating crack-driving forces in FGMs accurately and efficiently. Consequently, various numerical methods have been developed or examined to calculate stress-intensity factors (SIFs), such as the displacement correlation method and the modified crack-closure integral method (Kim and Paulino, 2002). Recently, Rao and Rahman (2003a,b) developed two new interaction integrals for the mixed-mode fracture analysis of cracks in both isotropic and orthotropic FGMs. In contrast to existing methods, it is not necessary to perform integration along the crack face of the discontinuity. Hence, the interaction integral method is simpler and more efficient than previously developed methods. Nevertheless, the majority of current numerical methods for orthotropic FGM fracture analysis stem from extensions to methods originally developed for cracks in homogeneous orthotropic materials.

An alternative approach to previously developed methods involves shape sensitivity analysis, which is frequently employed in structural design optimization. Shape sensitivity analysis permits direct, analytical evaluation of first-order (and higher-order, if required) derivatives of potential energy with respect to crack size. Broadly speaking, there are two fundamentally different approaches to shape sensitivity analysis. The first, known as the discrete approach, employs a discretized numerical model (e.g., finite element method [FEM], boundary element method [BEM], meshfree method, etc.) to approximate the potential energy and then transforms shape derivatives into differentiations of algebraic equations by controlling node motions. The second, known as the continuum approach and adopted in the present work, relies on the variational formulation used in continuum mechanics (Gurtin, 1981). In the latter approach, shape sensitivity analysis is conducted by introducing a smooth velocity field to simulate shape change of the initial domain due to the crack advance. While discrete and continuum approaches are related (the former is an approximation of the latter), the continuum approach has two principal advantages: (1) a rigorous mathematical theory is obtained, without the uncertainty/errors associated with finite-dimensional approximation errors; and (2) explicit relations for sensitivity are obtained in terms of physical quantities rather than in terms of sums of derivatives of element matrices. These characteristic features of the continuum approach are of major importance in developing structural optimization theory (Céa, 1981; Haug et al., 1986).

For homogeneous materials, several shape sensitivity methods involving discrete (Fuenmayor et al., 1997; Hwang et al., 1998; Giner et al., 2002) and continuum (Feijóo et al., 2000; Taroco, 2000; Lee and Grosse, 1993; Bonnet, 2001) formulations have appeared in calculating SIFs. Both FEM and BEM have been employed for the shape sensitivity analysis of cracks. Most of these investigations are applicable only to linear-elastic fracture-mechanics problems. More recently, continuum shape sensitivity methods have also been developed for predicting first-order sensitivities of mixed-mode

SIFs for isotropic materials (Chen et al., 2002, 2001a,b). These analytical sensitivities of SIFs provide a convenient means by which subsequent fracture reliability analysis can be performed accurately and efficiently. However, all of the aforementioned shape sensitivity methods are strictly applicable to homogeneous materials. As a result, there is considerable interest in developing shape sensitivity methods for the numerical evaluation of crack-driving forces in FGM. With this need in mind, the authors recently developed a continuum shape sensitivity method for calculating mixed-mode SIFs for a stationary crack in two-dimensional, linear-elastic, isotropic FGMs of arbitrary geometry (Rao and Rahman, submitted for publication). The main objective of present work is to extend that continuum shape sensitivity method for the numerical evaluation of crack-driving forces in orthotropic FGMs.

This paper presents a continuum shape sensitivity method for calculating mixed-mode SIFs for a stationary crack in two-dimensional, linear-elastic, orthotropic FGMs of arbitrary geometry. The method involves using the material derivative concept from continuum mechanics, the mutual potential energy release rate, and direct differentiation. Since the governing variational equation is differentiated prior to discretization, resulting sensitivity equations are independent of approximate numerical techniques, such as FEM, BEM, the mesh-free method, or others. Three numerical examples in conjunction with FEM are presented to evaluate the accuracy of fracture parameters calculated by the proposed method. Comparisons have been made between the SIFs predicted by the proposed method and available reference solutions in the literature, generated either analytically or numerically using various other fracture integrals or analyses.

2. Crack tip fields in FGM

Consider a plane problem in rectilinear anisotropic elasticity. The generalized Hooke's law for stress–strain relationship is given by

$$\varepsilon_i = \sum_{j=1}^{6} a_{ij}\sigma_j, \quad i,j = 1,2,\ldots,6, \tag{1}$$

where the compliance coefficients a_{ij}, with $a_{ij} = a_{ji}$, are contracted notations of the compliance tensor S_{ijkl} and

$$\begin{aligned} &\varepsilon_1 = \varepsilon_{11}, \quad \varepsilon_2 = \varepsilon_{22}, \quad \varepsilon_3 = \varepsilon_{33},\\ &\varepsilon_4 = 2\varepsilon_{23}, \quad \varepsilon_5 = 2\varepsilon_{13}, \quad \varepsilon_6 = 2\varepsilon_{12},\\ &\sigma_1 = \sigma_{11}, \quad \sigma_2 = \sigma_{22}, \quad \sigma_3 = \sigma_{33},\\ &\sigma_4 = \sigma_{23}, \quad \sigma_5 = \sigma_{13}, \quad \sigma_6 = \sigma_{12}. \end{aligned} \tag{2}$$

The compliance coefficients in Eq. (2) are a_{ij}, $i,j = 1, 2, 6$, for plane stress conditions, and the a_{ij} coefficients are exchanged with b_{ij} where $b_{ij} = a_{ij} - \frac{a_{i2}a_{j3}}{a_{33}}$, $i,j = 1, 2, 6$, for plane strain conditions.

Fig. 1 shows a crack tip that is referred to the Cartesian coordinate system in orthotropic FGMs. Two-dimensional anisotropic elasticity problems can be formulated in terms of the analytic functions $\phi_j(z_j)$ of the complex variable $z_j = x_j + \mathrm{i}y_j$ ($j = 1, 2$), where

$$x_j = x + \alpha_j y, \quad y_j = \beta_j y \qquad (j = 1,2). \tag{3}$$

The parameters α_j and β_j are the real and imaginary parts of $\mu_j = \alpha_j + \mathrm{i}\beta_j$, which can be determined from (Lekhnitskii et al., 1986)

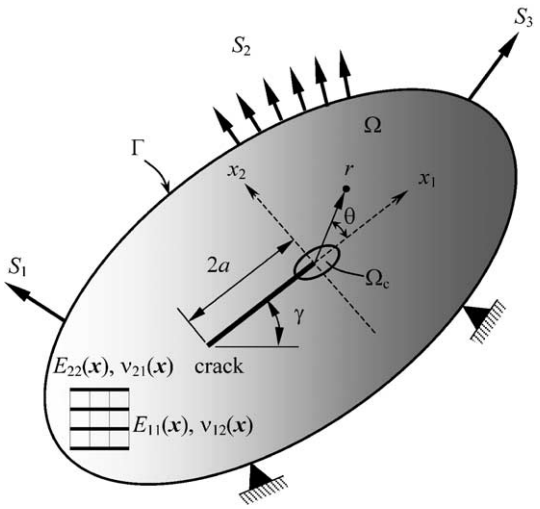

Fig. 1. A crack in an orthotropic functionally graded material.

$$a_{11}\mu^4 - 2a_{16}\mu^3 + (2a_{12} + a_{66})\mu^2 - 2a_{26}\mu + a_{22} = 0. \tag{4}$$

The roots μ_j are always either complex or purely imaginary in conjugate pairs as μ_1, $\bar{\mu}_1$, μ_2, and $\bar{\mu}_2$. Hence, the linear-elastic singular stress field near the crack tip can be obtained as (Shih et al., 1965)

$$\begin{aligned}\sigma_{11} = {} & \frac{K_{\mathrm{I}}}{\sqrt{2\pi r}}\mathrm{Re}\left[\frac{\mu_1\mu_2}{\mu_1-\mu_2}\left(\frac{\mu_2}{\sqrt{\cos\theta+\mu_2\sin\theta}}\right.\right.\\ & \left.\left.-\frac{\mu_1}{\sqrt{\cos\theta+\mu_1\sin\theta}}\right)\right]\\ & +\frac{K_{\mathrm{II}}}{\sqrt{2\pi r}}\mathrm{Re}\left[\frac{1}{\mu_1-\mu_2}\left(\frac{\mu_2^2}{\sqrt{\cos\theta+\mu_2\sin\theta}}\right.\right.\\ & \left.\left.-\frac{\mu_1^2}{\sqrt{\cos\theta+\mu_1\sin\theta}}\right)\right],\end{aligned} \tag{5}$$

$$\begin{aligned}\sigma_{22} = {} & \frac{K_{\mathrm{I}}}{\sqrt{2\pi r}}\mathrm{Re}\left[\frac{1}{\mu_1-\mu_2}\left(\frac{\mu_1}{\sqrt{\cos\theta+\mu_2\sin\theta}}\right.\right.\\ & \left.\left.-\frac{\mu_2}{\sqrt{\cos\theta+\mu_1\sin\theta}}\right)\right]\\ & +\frac{K_{\mathrm{II}}}{\sqrt{2\pi r}}\mathrm{Re}\left[\frac{1}{\mu_1-\mu_2}\left(\frac{1}{\sqrt{\cos\theta+\mu_2\sin\theta}}\right.\right.\\ & \left.\left.-\frac{1}{\sqrt{\cos\theta+\mu_1\sin\theta}}\right)\right],\end{aligned} \tag{6}$$

$$\begin{aligned}\sigma_{12} = {} & \frac{K_{\mathrm{I}}}{\sqrt{2\pi r}}\mathrm{Re}\left[\frac{\mu_1\mu_2}{\mu_1-\mu_2}\left(\frac{1}{\sqrt{\cos\theta+\mu_1\sin\theta}}\right.\right.\\ & \left.\left.-\frac{1}{\sqrt{\cos\theta+\mu_2\sin\theta}}\right)\right]\\ & +\frac{K_{\mathrm{II}}}{\sqrt{2\pi r}}\mathrm{Re}\left[\frac{1}{\mu_1-\mu_2}\left(\frac{\mu_1}{\sqrt{\cos\theta+\mu_1\sin\theta}}\right.\right.\\ & \left.\left.-\frac{\mu_2}{\sqrt{\cos\theta+\mu_2\sin\theta}}\right)\right].\end{aligned} \tag{7}$$

The near tip displacement field $\boldsymbol{z} = \{z_1, z_2\}^{\mathrm{T}}$ can be obtained as (Shih et al., 1965)

$$\begin{aligned}z_1 = {} & K_{\mathrm{I}}\sqrt{\frac{2r}{\pi}}\mathrm{Re}\left[\frac{1}{\mu_1-\mu_2}\left(\mu_1 p_2\sqrt{\cos\theta+\mu_2\sin\theta}\right.\right.\\ & \left.\left.-\mu_2 p_1\sqrt{\cos\theta+\mu_1\sin\theta}\right)\right]\\ & +K_{\mathrm{II}}\sqrt{\frac{2r}{\pi}}\mathrm{Re}\left[\frac{1}{\mu_1-\mu_2}\left(p_2\sqrt{\cos\theta+\mu_2\sin\theta}\right.\right.\\ & \left.\left.-p_1\sqrt{\cos\theta+\mu_1\sin\theta}\right)\right],\end{aligned} \tag{8}$$

and

$$\begin{aligned}z_2 = {} & K_{\mathrm{I}}\sqrt{\frac{2r}{\pi}}\mathrm{Re}\left[\frac{1}{\mu_1-\mu_2}\left(\mu_1 q_2\sqrt{\cos\theta+\mu_2\sin\theta}\right.\right.\\ & \left.\left.-\mu_2 q_1\sqrt{\cos\theta+\mu_1\sin\theta}\right)\right]\\ & +K_{\mathrm{II}}\sqrt{\frac{2r}{\pi}}\mathrm{Re}\left[\frac{1}{\mu_1-\mu_2}\left(q_2\sqrt{\cos\theta+\mu_2\sin\theta}\right.\right.\\ & \left.\left.-q_1\sqrt{\cos\theta+\mu_2\sin\theta}\right)\right].\end{aligned} \tag{9}$$

In Eqs. (5)–(9), μ_1 and μ_2 denote the crack-tip parameters calculated as the roots of Eq. (4), which are taken such that $\beta_j > 0$ ($j = 1, 2$), and p_j and q_j are given by

$$p_j = a_{11}\mu_j^2 + a_{12} - a_{16}\mu_j, \tag{10}$$

$$q_j = a_{12}\mu_j + \frac{a_{22}}{\mu_j} - a_{26}. \tag{11}$$

Even though the material gradient does not influence the square-root singularity or the singular stress distribution, the material gradient does affect the SIFs. Hence, the fracture parameters are functions of the material gradients, external loading, and geometry.

3. Shape sensitivity analysis

3.1. Velocity field

Consider a general three-dimensional body with a specific configuration, referred to as the initial (reference) configuration, with domain Ω, boundary Γ, and a body material point identified by position vector $\boldsymbol{x} \in \Omega$. Consider the motion of the body from an initial configuration with domain Ω and boundary Γ into a perturbed configu-

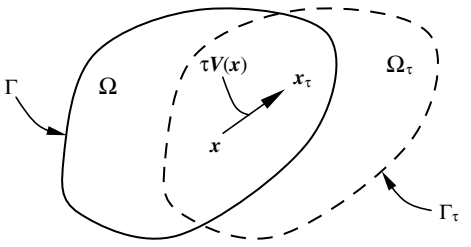

Fig. 2. Variation of domain.

ration with domain Ω_τ and boundary Γ_τ, as shown in Fig. 2. This process can be expressed as

$$\boldsymbol{T} : \boldsymbol{x} \to \boldsymbol{x}_\tau, \quad \boldsymbol{x} \in \Omega, \tag{12}$$

where $\boldsymbol{x}_\tau$ is the position vector of the material point in the perturbed configuration, $\boldsymbol{T}$ is a transformation mapping, and $\tau \in \mathbb{R}^+$ is a scalar, fictitious, time-like parameter denoting the amount of shape change, with

$$\begin{aligned} \boldsymbol{x}_\tau &= \boldsymbol{T}(\boldsymbol{x}, \tau), \\ \Omega_\tau &= \boldsymbol{T}(\Omega, \tau), \\ \Gamma_\tau &= \boldsymbol{T}(\Gamma, \tau). \end{aligned} \tag{13}$$

A velocity field can then be defined as

$$\boldsymbol{v}(\boldsymbol{x}_\tau, \tau) \equiv \frac{\mathrm{d}\boldsymbol{x}_\tau}{\mathrm{d}\tau} = \frac{\mathrm{d}\boldsymbol{T}(\boldsymbol{x}, \tau)}{\mathrm{d}\tau} = \frac{\partial \boldsymbol{T}(\boldsymbol{x}, \tau)}{\partial \tau}. \tag{14}$$

In the neighborhood of the initial time $\tau = 0$, assuming a regularity hypothesis and ignoring high-order terms,

$$\begin{aligned} \boldsymbol{x}_\tau = \boldsymbol{T}(\boldsymbol{x}, \tau) &= \boldsymbol{T}(\boldsymbol{x}, 0) + \tau \frac{\partial \boldsymbol{T}(\boldsymbol{x}, 0)}{\partial \tau} + \mathrm{O}(\tau^2) \\ &\cong \boldsymbol{x} + \tau \boldsymbol{v}(\boldsymbol{x}, 0), \end{aligned} \tag{15}$$

where $\boldsymbol{x} = \boldsymbol{T}(\boldsymbol{x}, 0)$. For the rest of this paper, the velocity field $\boldsymbol{v}(\boldsymbol{x}, 0)$ will be denoted by $\boldsymbol{V}(x)$ or $\boldsymbol{V}$. Thus, a velocity field characterizes the direction of domain variation, which implies that for a given $\boldsymbol{V}(\boldsymbol{x})$, the shape change of Ω is uniquely controlled by the scalar parameter τ.

3.2. Sensitivity analysis

The variational governing equation for a linear-elastic, non-homogeneous or homogeneous orthotropic solid with domain Ω can be formulated as (Haug et al., 1986)

$$a_\Omega(\boldsymbol{z}, \bar{z}) = \ell_\Omega(\bar{\boldsymbol{z}}) \quad \text{for all } \bar{z} \in \boldsymbol{Z}, \tag{16}$$

where $\boldsymbol{z}$ and $\bar{\boldsymbol{z}}$ are the actual and virtual displacement fields of the structure, respectively, $\boldsymbol{Z}$ is the space of kinematically admissible virtual displacements, and $a_\Omega(\boldsymbol{z}, \bar{\boldsymbol{z}})$ and $\ell_\Omega(\bar{\boldsymbol{z}})$ are energy bilinear and load linear forms, respectively. The subscript Ω in Eq. (16) is used to indicate the dependency of the governing equation on the shape of the structural domain. If $\boldsymbol{z}_\tau(\boldsymbol{x}_\tau)$ represents the displacement at $\boldsymbol{x}_\tau = \boldsymbol{x} + \tau \boldsymbol{V}(x)$ of the perturbed domain, the pointwise material derivative at $x \in \Omega$ is defined as (Haug et al., 1986)

$$\begin{aligned} \dot{\boldsymbol{z}}(\boldsymbol{x}) &\equiv \lim_{\tau \to 0} \left[\frac{\boldsymbol{z}_\tau(\boldsymbol{x} + \tau \boldsymbol{V}(\boldsymbol{x})) - \boldsymbol{z}(\boldsymbol{x})}{\tau} \right] \\ &= \boldsymbol{z}'(\boldsymbol{x}) + \nabla \boldsymbol{z}^T \boldsymbol{V}(\boldsymbol{x}), \end{aligned} \tag{17}$$

where

$$\boldsymbol{z}' = \lim_{\tau \to 0} \left[\frac{\boldsymbol{z}_\tau(\boldsymbol{x}) - \boldsymbol{z}(\boldsymbol{x})}{\tau} \right] \tag{18}$$

is the partial derivative of $\boldsymbol{z}$ and $\nabla = \{\partial/\partial x_1, \partial/\partial x_2, \partial/\partial x_3\}^{\mathrm{T}}$ is the vector of gradient operators.

If no body forces are involved, the variational equation (Eq. (16)) can be written as

$$\begin{aligned} a_\Omega(\boldsymbol{z}, \bar{\boldsymbol{z}}) &\equiv \int_\Omega \sigma_{ij}(\boldsymbol{z}) \varepsilon_{ij}(\bar{\boldsymbol{z}}) \, \mathrm{d}\Omega = \ell_\Omega(\bar{\boldsymbol{z}}) \\ &\equiv \int_\Omega T_i \bar{z}_i \, \mathrm{d}\Gamma, \end{aligned} \tag{19}$$

where $\sigma_{ij}(\boldsymbol{z})$ and $\varepsilon_{ij}(\bar{\boldsymbol{z}})$ are components of the stress and strain tensors of the displacement $\boldsymbol{z}$ and virtual displacement $\bar{\boldsymbol{z}}$, respectively, T_i is the ith component of the surface traction, and $\bar{z}_i$ is the ith component of $\bar{\boldsymbol{z}}$. Taking the material derivative of both sides of Eq. (19), it can be shown that (Haug et al., 1986)

$$a_\Omega(\dot{\boldsymbol{z}}, \bar{\boldsymbol{z}}) = \ell'_{\boldsymbol{V}}(\bar{\boldsymbol{z}}) - a'_{\boldsymbol{V}}(\boldsymbol{z}, \bar{\boldsymbol{z}}) \quad \forall \bar{\boldsymbol{z}} \in \boldsymbol{Z}, \tag{20}$$

where the subscript $\boldsymbol{V}$ indicates the dependency of the terms on the velocity field. The terms $\ell'_{\boldsymbol{V}}(\bar{\boldsymbol{z}})$ and $a'_{\boldsymbol{V}}(\boldsymbol{z}, \bar{\boldsymbol{z}})$ can be further derived as (Haug et al., 1986)

$$\begin{aligned} \ell'_{\boldsymbol{V}}(\bar{\boldsymbol{z}}) = \int_\Gamma \{ &-T_i(\bar{z}_{i,j} V_j) + [(T_i \bar{z}_i)_{,j} n_j \\ &+ \kappa_\Gamma (T_i \bar{z}_i)](V_i n_i) \} \mathrm{d}\Gamma \end{aligned} \tag{21}$$

and

$$a'_{\boldsymbol{V}}(\boldsymbol{z},\bar{\boldsymbol{z}}) = -\int_{\Omega}\big[\varepsilon_{ij}(\boldsymbol{z})D_{ijkl}(\boldsymbol{x})(\bar{z}_{k,m}V_{m,l}) + \varepsilon_{ij}(\bar{\boldsymbol{z}})D_{ijkl}(\boldsymbol{x})(z_{k,m}V_{m,l}) - \varepsilon_{ij}(\bar{\boldsymbol{z}})D_{ijkl,m}(\boldsymbol{x})\varepsilon_{kl}(\boldsymbol{z})V_m - \varepsilon_{ij}(\boldsymbol{z})D_{ijkl}(\boldsymbol{x})\varepsilon_{kl}(\bar{\boldsymbol{z}})\mathrm{div}\boldsymbol{V}\big]\mathrm{d}\Omega, \tag{22}$$

where n_i is the ith component of unit normal vector $\boldsymbol{n}$, κ_Γ is the curvature of the boundary, $z_{i,j} = \partial z_i/\partial x_j$, $\bar{z}_{i,j} = \partial \bar{z}_i/\partial x_j$, $V_{i,j} = \partial V_i/\partial x_j$, $D_{ijkl}(\boldsymbol{x})$ is a component of the constitutive tensor given by $D_{ijkl}(\boldsymbol{x}) = S^{-1}_{ijkl}(\boldsymbol{x})$ and $D_{ijkl,m}(\boldsymbol{x}) = \partial D_{ijkl}(\boldsymbol{x})/\partial x_m$. Notice that the third term in the integrand on the right-hand side of Eq. (22) arises naturally in the formulation of continuum shape sensitivity analysis for non-homogeneous orthotropic materials, but vanishes for homogeneous orthotropic materials. Also, D_{ijkl} is constant for a homogeneous orthotropic material.

4. Shape sensitivity method for fracture analysis

In this section, continuum shape sensitivity method for homogeneous orthotropic materials is briefly summarized, and then it is extended for cracks in orthotropic FGM, which is the main objective of present work. The study of orthotropic FGM should enhance the understanding of a fracture in a generic material, since upon shrinking, the gradient layer in FGM is expected to behave like a sharp interface, and upon expansion the fracture behavior would be analogous to that of a homogeneous orthotropic material.

4.1. Homogeneous materials

Consider an arbitrary, two-dimensional cracked body of crack length a, with unit thickness subjected to an arbitrary loading. The total potential energy Π of the system in the absence of body forces is

$$\Pi \equiv \frac{1}{2}\int_{\Omega}\varepsilon_{ij}(\boldsymbol{z})D_{ijkl}\varepsilon_{kl}(\boldsymbol{z})\,\mathrm{d}\Omega - \int_{\Gamma}T_i z_i\,\mathrm{d}\Gamma, \tag{23}$$

where, for two-dimensional linear elastic material models, D_{ijkl}, are the components of the constant elasticity matrix.

By substituting $\bar{\boldsymbol{z}}$ with $\boldsymbol{z}$ in Eq. (19) and by using Eq. (23), the following is produced:

$$\Pi = -\tfrac{1}{2}a_{\Omega}(\boldsymbol{z},\boldsymbol{z}). \tag{24}$$

The energy release rate is equal to the derivative of potential energy with respect to the crack area. For a two-dimensional cracked structure with unit thickness, the crack area is equal to crack length a. Assuming crack length a to be the variable of interest, a change in crack area or crack length involves a change in the shape of the cracked continuum. In relation to shape sensitivity theory, such a change implies that the energy release rate is equal to the material derivative of potential energy. Hence, for elastic (linear or nonlinear) solids under mixed-mode loading conditions, the J-integral, which is equal to the energy release rate, can be derived as

$$J \equiv -\dot{\Pi} = \tfrac{1}{2}[a_{\Omega}(\dot{\boldsymbol{z}},\boldsymbol{z}) + a_{\Omega}(\boldsymbol{z},\dot{\boldsymbol{z}}) + a'_{\boldsymbol{V}}(\boldsymbol{z},\boldsymbol{z})], \tag{25}$$

where the overdot indicates a material derivative. If (1) velocity field $\boldsymbol{V}(\boldsymbol{x})$ is defined such that traction-loading boundary Γ is fixed, i.e., $\boldsymbol{V}(\boldsymbol{x}) = 0$ on the traction-loading boundary Γ; and (2) $\bar{\boldsymbol{z}}$ is replaced with $\boldsymbol{z}$ in Eq. (20), noting that $a_{\Omega}(\dot{\boldsymbol{z}},\boldsymbol{z}) = a_{\Omega}(\boldsymbol{z},\dot{\boldsymbol{z}}) = -a'_{\boldsymbol{V}}(\boldsymbol{z},\boldsymbol{z})$, then

$$J = -\tfrac{1}{2}a'_{\boldsymbol{V}}(\boldsymbol{z},\boldsymbol{z}). \tag{26}$$

Substituting the expression of $a'_{\boldsymbol{V}}(\boldsymbol{z},\boldsymbol{z})$ from Eq. (22) and noting that D_{ijkl} is constant for homogeneous materials ($D_{ijkl,m} = 0$) gives

$$J = \frac{1}{2}\int_{\Omega}[\sigma_{ij}(\boldsymbol{z})(z_{i,k}V_{k,j}) + \sigma_{ij}(\boldsymbol{z})(z_{i,k}V_{k,j}) - \sigma_{ij}(\boldsymbol{z})\varepsilon_{ij}(\boldsymbol{z})\mathrm{div}\boldsymbol{V}]\mathrm{d}\Omega. \tag{27}$$

Defining $W = \sigma_{ij}\varepsilon_{ij}/2$ as the strain energy density and $\boldsymbol{V}(\boldsymbol{x}) = \{V_1(\boldsymbol{x}), 0\}^{\mathrm{T}}$ as the velocity field, with $V_1(\boldsymbol{x})$ having a value of *unity* at the crack tip, *zero* along the boundary of the domain, and arbitrary elsewhere, the following is produced:

$$J = \int_{\Omega}\left(\sigma_{ij}\frac{\partial z_i}{\partial x_i} - W\delta_{1j}\right)\frac{\partial V_1}{\partial x_j}\mathrm{d}\Omega \tag{28}$$

which is the same as the traditional domain form of the J-integral, with V_1 taking the place of *weight function* q. Hence, weight function q can be consid-

ered the virtual change in crack length, having a value of *unity* at the crack tip, *zero* along the boundary of the domain, and arbitrary elsewhere.

Now, consider two independent equilibrium states of the cracked body. Let state 1 correspond to the *actual* state for given boundary conditions, and let state 2 correspond to an *auxiliary* state, which can be either mode-I or mode-II near crack tip displacement and stress fields for homogeneous materials (Rao and Rahman, 2003a,b). Superposition of these two states leads to another equilibrium state (state S) for which the total potential energy $\Pi^{(S)}$ is

$$\Pi^{(S)} = \frac{1}{2} - \int_{\Omega} \varepsilon_{ij}(\boldsymbol{z}^{(1)} + \boldsymbol{z}^{(2)}) D_{ijkl} \varepsilon_{kl}(\boldsymbol{z}^{(1)} + \boldsymbol{z}^{(2)})\, \mathrm{d}\Omega - \int_{\Gamma} (T_i^{(1)} + T_i^{(2)})(z_i^{(1)} + z_i^{(2)})\, \mathrm{d}\Gamma, \tag{29}$$

where $z_i^{(1)}$, $T_i^{(1)}$ are the components of displacement and external force vectors, respectively, of the *actual* state for given boundary conditions, and $z_i^{(2)}$, $T_i^{(2)}$ are the components of displacement and external force vectors, respectively, of the *auxiliary* state. By using the divergence theorem,

$$\int_{\Gamma} (T_i^{(1)})(z_i^{(1)})\, \mathrm{d}\Gamma = \int_{\Omega} \varepsilon_{ij}(\boldsymbol{z}^{(1)}) D_{ijkl} \varepsilon_{kl}(\boldsymbol{z}^{(1)})\, \mathrm{d}\Omega, \tag{30}$$

$$\int_{\Gamma} (T_i^{(2)})(z_i^{(2)})\, \mathrm{d}\Gamma = \int_{\Omega} \varepsilon_{ij}(\boldsymbol{z}^{(2)}) D_{ijkl} \varepsilon_{kl}(\boldsymbol{z}^{(2)})\, \mathrm{d}\Omega, \tag{31}$$

$$\int_{\Gamma} (T_i^{(1)})(z_i^{(2)})\, \mathrm{d}\Gamma = \int_{\Omega} \varepsilon_{ij}(\boldsymbol{z}^{(1)}) D_{ijkl} \varepsilon_{kl}(\boldsymbol{z}^{(2)})\, \mathrm{d}\Omega, \tag{32}$$

and

$$\int_{\Gamma} (T_i^{(2)})(z_i^{(1)})\, \mathrm{d}\Gamma = \int_{\Omega} \varepsilon_{ij}(\boldsymbol{z}^{(2)}) D_{ijkl} \varepsilon_{kl}(\boldsymbol{z}^{(1)})\, \mathrm{d}\Omega, \tag{33}$$

which, when applied to the expanded form of Eq. (29) yields

$$\Pi^{(S)} = \Pi^{(1)} + \Pi^{(2)} + \Pi^{(1,2)}, \tag{34}$$

where

$$\Pi^{(1)} = -\tfrac{1}{2} a_{\Omega}(\boldsymbol{z}^{(1)}, \boldsymbol{z}^{(1)}), \tag{35}$$

$$\Pi^{(2)} = -\tfrac{1}{2} a_{\Omega}(\boldsymbol{z}^{(2)}, \boldsymbol{z}^{(2)}), \tag{36}$$

and

$$\Pi^{(1,2)} = -\tfrac{1}{2} a_{\Omega}(\boldsymbol{z}^{(1)}, \boldsymbol{z}^{(2)}) - \tfrac{1}{2} a_{\Omega}(\boldsymbol{z}^{(2)}, \boldsymbol{z}^{(1)}) \tag{37}$$

are various potential energies with

$$a_{\Omega}(\boldsymbol{z}^{(i)}, \boldsymbol{z}^{(j)}) = \int_{\Omega} \varepsilon_{ij}(z^{(i)}) D_{ijkl} \varepsilon_{kl}(z^{(j)})\, \mathrm{d}\Omega; \quad i, j = 1, 2. \tag{38}$$

Hence, the J-integral for the superposed state, denoted by $J^{(S)}$, can be obtained as

$$J^{(S)} \equiv -\dot{\Pi}^{(S)} = -\dot{\Pi}^{(1)} - \dot{\Pi}^{(2)} - \dot{\Pi}^{(1,2)}. \tag{39}$$

Again, if the velocity field is defined such that $\boldsymbol{V}(\boldsymbol{x}) = \boldsymbol{0}$ on the traction-loading boundary Γ and under similar considerations, $a_{\Omega}(\boldsymbol{z}^{(i)}, \boldsymbol{z}^{(j)}) = a_{\Omega}(\boldsymbol{z}^{(i)}, \boldsymbol{z}^{(j)}) = -a'_{\boldsymbol{V}}(\boldsymbol{z}^{(i)}, \boldsymbol{z}^{(j)})$; $i, j = 1, 2$, yielding

$$J^{(S)} = -\tfrac{1}{2} a'_{\boldsymbol{V}}(\boldsymbol{z}^{(1)}, \boldsymbol{z}^{(1)}) - \tfrac{1}{2} a'_{\boldsymbol{V}}(\boldsymbol{z}^{(2)}, \boldsymbol{z}^{(2)}) - \tfrac{1}{2} a'_{\boldsymbol{V}}(\boldsymbol{z}^{(1)}, \boldsymbol{z}^{(2)}) - \tfrac{1}{2} a'_{\boldsymbol{V}}(\boldsymbol{z}^{(2)}, \boldsymbol{z}^{(1)}). \tag{40}$$

On further expansion, $J^{(S)}$ can be decomposed to

$$J^{(S)} = J^{(1)} + J^{(2)} + M^{(1,2)}, \tag{41}$$

where

$$J^{(1)} = -\dot{\Pi}^{(1)} = -\tfrac{1}{2} a'_{\boldsymbol{V}}(\boldsymbol{z}^{(1)}, \boldsymbol{z}^{(1)}) \tag{42}$$

and

$$J^{(2)} = -\dot{\Pi}^{(2)} = -\tfrac{1}{2} a'_{\boldsymbol{V}}(\boldsymbol{z}^{(2)}, \boldsymbol{z}^{(2)}) \tag{43}$$

are the J-integrals for states 1 and 2, respectively, noting that $a'_{\boldsymbol{V}}(\boldsymbol{z}^{(1)}, \boldsymbol{z}^{(2)}) = a'_{\boldsymbol{V}}(\boldsymbol{z}^{(2)}, \boldsymbol{z}^{(1)})$,

$$M^{(1,2)} = -\dot{\Pi}^{(1,2)} = -a'_{\boldsymbol{V}}(\boldsymbol{z}^{(1)}, \boldsymbol{z}^{(2)}) \tag{44}$$

is the mutual potential energy release rate. By replacing z, and $\bar{z}$ in Eq. (22) with $\boldsymbol{z}^{(1)}$, and $\boldsymbol{z}^{(2)}$ respectively, and assuming $\boldsymbol{V}(\boldsymbol{x})$ with $V_1(x)$ having a value of unity at the crack tip, zero along the boundary of the domain, and arbitrary elsewhere, the following is obtained:

$$M^{(1,2)} = \int_{\Omega} \left[\sigma_{ij}(\boldsymbol{z}^{(1)}) \frac{\partial z_i^{(2)}}{\partial x_1} + \sigma_{ij}(\boldsymbol{z}^{(2)}) \frac{\partial z_i^{(1)}}{\partial x_1} - W^{(1,2)} \delta_{1j} \right] \frac{\partial V_1}{\partial x_j}\, \mathrm{d}\Omega, \tag{45}$$

where $W^{(1,2)} = [\sigma_{ij}(\boldsymbol{z}^{(1)}) \varepsilon_{ij}(\boldsymbol{z}^{(2)}) + \sigma_{ij}(\boldsymbol{z}^{(2)}) \varepsilon_{ij}(\boldsymbol{z}^{(1)})]/2$ is the mutual strain energy density. Again, $M^{(1,2)}$ in Eq. (45) is same as the domain form of the M-integral (interaction integral) for the mixed-mode

fracture of homogeneous materials, with V_1 taking the place of *weight function q*. In fact, various fracture integrals can be derived using shape sensitivity analysis.

4.2. Functionally graded materials

As with the treatment of homogeneous materials, consider two independent equilibrium states of an FGM cracked structure. Let state 1 correspond to the *actual* state for given boundary conditions. Let state 2 correspond to an *auxiliary* state, which can be either mode-I or mode-II near tip displacement and stress fields. Superposition of these two states leads to another equilibrium state (state S) for which the total potential energy, henceforth referred to as $\tilde{\Pi}^{(S)}$, is

$$\tilde{\Pi}^{(S)} = \frac{1}{2}\int_{\Omega} \varepsilon_{ij}(\boldsymbol{z}^{(1)}+\boldsymbol{z}^{(2)})D_{ijkl}(\boldsymbol{x})\varepsilon_{kl}(\boldsymbol{z}^{(1)}+\boldsymbol{z}^{(2)})\,\mathrm{d}\Omega - \int_{\Gamma}(T_i^{(1)}+T_i^{(2)})(\boldsymbol{z}_i^{(1)}+\boldsymbol{z}_i^{(2)})\,\mathrm{d}\Gamma. \tag{46}$$

For states 1 and S, $D_{ijkl}(\boldsymbol{x})$ varies as the function of spatial location. However, for state 2, which is the auxiliary state, a different constitutive matrix that satisfies both equilibrium and compatibility conditions must be defined. For state 2, define a $D^{\mathrm{aux}}_{ijkl}(\boldsymbol{x})$ that can be obtained from the elastic constants evaluated at the crack tip. The divergence theorem yields

$$\int_{\Gamma}(T_i^{(1)})(z_i^{(1)})\,\mathrm{d}\Gamma = \int_{\Omega}\varepsilon_{ij}(\boldsymbol{z}^{(1)})D_{ijkl}(\boldsymbol{x})\varepsilon_{kl}(\boldsymbol{z}^{(1)})\,\mathrm{d}\Omega, \tag{47}$$

$$\int_{\Gamma}(T_i^{(2)})(z_i^{(2)})\,\mathrm{d}\Gamma = \int_{\Omega}\varepsilon_{ij}(\boldsymbol{z}^{(2)})D_{ijkl}(\boldsymbol{x})\varepsilon_{kl}(\boldsymbol{z}^{(2)})\,\mathrm{d}\Omega, \tag{48}$$

$$\int_{\Gamma}(T_i^{(1)})(z_i^{(2)})\,\mathrm{d}\Gamma = \int_{\Omega}\varepsilon_{ij}(\boldsymbol{z}^{(1)})D_{ijkl}(\boldsymbol{x})\varepsilon_{kl}(\boldsymbol{z}^{(2)})\,\mathrm{d}\Omega, \tag{49}$$

and

$$\int_{\Gamma}(T_i^{(2)})(z_i^{(1)})\,\mathrm{d}\Gamma = \int_{\Omega}\varepsilon_{ij}(\boldsymbol{z}^{(2)})D_{ijkl}(\boldsymbol{x})\varepsilon_{kl}(\boldsymbol{z}^{(1)})\,\mathrm{d}\Omega, \tag{50}$$

which, when applied to the expanded form of Eq. (46), gives

$$\tilde{\Pi}^{(S)} = \tilde{\Pi}^{(1)} + \tilde{\Pi}^{(2)} + \tilde{\Pi}^{(1,2)}, \tag{51}$$

where

$$\tilde{\Pi}^{(1)} = -\tfrac{1}{2}a_{\Omega}(\boldsymbol{z}^{(1)},\boldsymbol{z}^{(1)}), \tag{52}$$

$$\tilde{\Pi}^{(2)} = -\tfrac{1}{2}a^{\mathrm{aux}}_{\Omega}(\boldsymbol{z}^{(2)},\boldsymbol{z}^{(2)}), \tag{53}$$

$$\tilde{\Pi}^{(1,2)} = -a_{\Omega}(\boldsymbol{z}^{(1)},\boldsymbol{z}^{(2)}) - \tfrac{1}{2}a_{\Omega}(\boldsymbol{z}^{(2)},\boldsymbol{z}^{(2)}) + \tfrac{1}{2}a^{\mathrm{aux}}_{\Omega}(\boldsymbol{z}^{(2)},\boldsymbol{z}^{(2)}), \tag{54}$$

with

$$a_{\Omega}(\boldsymbol{z}^{(1)},\boldsymbol{z}^{(2)}) = \int_{\Omega}\varepsilon_{ij}(\boldsymbol{z}^{(1)})D_{ijkl}(\boldsymbol{x})\varepsilon_{kl}(\boldsymbol{z}^{(2)})\,\mathrm{d}\Omega, \tag{55}$$

$$a_{\Omega}(\boldsymbol{z}^{(2)},\boldsymbol{z}^{(2)}) = \int_{\Omega}\varepsilon_{ij}(\boldsymbol{z}^{(2)})D_{ijkl}(\boldsymbol{x})\varepsilon_{kl}(\boldsymbol{z}^{(2)})\,\mathrm{d}\Omega, \tag{56}$$

and

$$a^{\mathrm{aux}}_{\Omega}(\boldsymbol{z}^{(2)},\boldsymbol{z}^{(2)}) = \int_{\Omega}\varepsilon_{ij}(\boldsymbol{z}^{(2)})D^{\mathrm{aux}}_{ijkl}\varepsilon_{kl}(\boldsymbol{z}^{(2)})\,\mathrm{d}\Omega. \tag{57}$$

Hence, the J-integral for the superposed state, denoted as $\tilde{J}^{(S)}$, can be obtained from

$$\tilde{J}^{(S)} \equiv -\dot{\tilde{\Pi}}^{(S)} = -\dot{\tilde{\Pi}}^{(1)} - \dot{\tilde{\Pi}}^{(2)} - \dot{\tilde{\Pi}}^{(1,2)}. \tag{58}$$

If the velocity field is defined such that $\boldsymbol{V}(\boldsymbol{x}) = \boldsymbol{0}$ on the traction-loading boundary Γ, then

$$a_{\Omega}(\boldsymbol{z}^{(1)},\boldsymbol{z}^{(2)}) = -a'_{\boldsymbol{V}}(\boldsymbol{z}^{(1)},\boldsymbol{z}^{(2)}),$$

$$a_{\Omega}(\boldsymbol{z}^{(2)},\boldsymbol{z}^{(2)}) = -a'_{\boldsymbol{V}}(\boldsymbol{z}^{(2)},\boldsymbol{z}^{(2)}),$$

and

$$a^{\mathrm{aux}}_{\Omega}(\boldsymbol{z}^{(2)},\boldsymbol{z}^{(2)}) = -a'^{\mathrm{aux}}_{\boldsymbol{V}}(\boldsymbol{z}^{(2)},\boldsymbol{z}^{(2)}).$$

Hence, $\tilde{J}^{(S)}$ can be decomposed into

$$\tilde{J}^{(S)} = \tilde{J}^{(1)} + \tilde{J}^{(2)} + \tilde{M}^{(1,2)}, \tag{59}$$

in which

$$\tilde{J}^{(1)} = -\dot{\tilde{\Pi}}^{(1)} = -\tfrac{1}{2}a'_{V}(\boldsymbol{z}^{(1)},\boldsymbol{z}^{(1)}), \tag{60}$$

$$\tilde{J}^{(2)} = -\dot{\tilde{\Pi}}^{(2)} = -\tfrac{1}{2}a'^{\mathrm{aux}}_{V}(\boldsymbol{z}^{(2)},\boldsymbol{z}^{(2)}) \tag{61}$$

are the $\tilde{J}$-integrals for states 1 and 2, respectively, and

$$\begin{aligned}\tilde{M}^{(1,2)} &= -\dot{\tilde{\Pi}}^{(1,2)} \\ &= -a'_V(\boldsymbol{z}^{(1)},\boldsymbol{z}^{(2)}) + \tfrac{1}{2}[a'^{\text{aux}}_V(\boldsymbol{z}^{(2)},\boldsymbol{z}^{(2)}) \\ &\quad - a'_V(\boldsymbol{z}^{(2)},\boldsymbol{z}^{(2)})] \end{aligned} \tag{62}$$

is the mutual potential energy release rate, where

$$\begin{aligned} a'_V(\boldsymbol{z}^{(1)},\boldsymbol{z}^{(1)}) = -\int_\Omega \Big[&\varepsilon_{ij}(z^{(1)})D_{ijkl}(\boldsymbol{x})(z^{(1)}_{k,m}V_{m,l}) \\ &+\varepsilon_{ij}(z^{(1)})D_{ijkl}(\boldsymbol{x})(z^{(1)}_{k,m}V_{m,l}) \\ &-\varepsilon_{ij}(z^{(1)})D_{ijkl,m}(\boldsymbol{x})\varepsilon_{kl}(z^{(1)})V_m \\ &-\varepsilon_{ij}(z^{(1)})D_{ijkl}(\boldsymbol{x})\varepsilon_{kl}(z^{(1)})\operatorname{div}\boldsymbol{V}\Big]\,\mathrm{d}\Omega, \end{aligned} \tag{63}$$

$$\begin{aligned} a'_V(\boldsymbol{z}^{(1)},\boldsymbol{z}^{(2)}) = -\int_\Omega \Big[&\varepsilon_{ij}(z^{(1)})D_{ijkl}(\boldsymbol{x})(z^{(2)}_{k,m}V_{m,l}) \\ &+\varepsilon_{ij}(z^{(2)})D_{ijkl}(\boldsymbol{x})(z^{(1)}_{k,m}V_{m,l}) \\ &-\varepsilon_{ij}(z^{(2)})D_{ijkl,m}(\boldsymbol{x})\varepsilon_{kl}(z^{(1)})V_m \\ &-\varepsilon_{ij}(z^{(1)})D_{ijkl}(\boldsymbol{x})\varepsilon_{kl}(z^{(2)})\operatorname{div}\boldsymbol{V}\Big]\,\mathrm{d}\Omega, \end{aligned} \tag{64}$$

$$\begin{aligned} a'^{\text{aux}}_V(\boldsymbol{z}^{(2)},\boldsymbol{z}^{(2)}) = -\int_\Omega \Big[&\varepsilon_{ij}(z^{(2)})D^{\text{aux}}_{ijkl}(\boldsymbol{x})(z^{(2)}_{k,m}V_{m,l}) \\ &+\varepsilon_{ij}(z^{(2)})D^{\text{aux}}_{ijkl}(\boldsymbol{x})(z^{(2)}_{k,m}V_{m,l}) \\ &-\varepsilon_{ij}(z^{(2)})D^{\text{aux}}_{ijkl}(\boldsymbol{x})\varepsilon_{kl}(z^{(2)})\operatorname{div}\boldsymbol{V}\Big]\,\mathrm{d}\Omega, \end{aligned} \tag{65}$$

and

$$\begin{aligned} a'_V(\boldsymbol{z}^{(2)},\boldsymbol{z}^{(2)}) = -\int_\Omega \Big[&\varepsilon_{ij}(z^{(2)})D_{ijkl}(\boldsymbol{x})(z^{(2)}_{k,m}V_{m,l}) \\ &+\varepsilon_{ij}(z^{(2)})D_{ijkl}(\boldsymbol{x})(z^{(2)}_{k,m}V_{m,l}) \\ &-\varepsilon_{ij}(z^{(2)})D_{ijkl,m}(\boldsymbol{x})\varepsilon_{kl}(z^{(2)})V_m \\ &-\varepsilon_{ij}(z^{(2)})D_{ijkl}(\boldsymbol{x})\varepsilon_{kl}(z^{(2)})\operatorname{div}\boldsymbol{V}\Big]\,\mathrm{d}\Omega. \end{aligned} \tag{66}$$

To evaluate all three terms of $\tilde{M}^{(1,2)}$ in Eq. (62), one needs to *prescribe* an appropriate velocity field $\boldsymbol{V}(\boldsymbol{x})$ and auxiliary displacement field $\boldsymbol{z}^{(2)}$; and *calculate* actual displacement field $\boldsymbol{z}^{(1)}$ for the initial shape of the cracked body. In other words, a single stress analysis employing a suitable numerical method, such as FEM or the mesh-free method, efficiently evaluates $\tilde{J}$- and $\tilde{M}$-integrals. In contrast to Eqs. (26) and (44), which lead to existing expressions of J- and M-integrals in homogeneous materials, respectively, Eq. (62) is new and applicable to general non-homogeneous materials. When both the elastic modulus and Poisson's ratio have no spatial variation, $a'^{\text{aux}}_V(\boldsymbol{z}^{(2)},\boldsymbol{z}^{(2)}) = a'_V(\boldsymbol{z}^{(2)},\boldsymbol{z}^{(2)})$, the $\tilde{J}$- and $\tilde{M}$-integrals in Eqs. (60)–(62) degenerate into homogeneous solutions, as expected.

4.3. Stress intensity factors

For linear-elastic solids, the $\tilde{J}$-integral also represents the energy release rate and, as a result,

$$\tilde{J} = \alpha_{11}K_{\text{I}}^2 + \alpha_{12}K_{\text{I}}K_{\text{II}} + \alpha_{22}K_{\text{II}}^2, \tag{67}$$

where

$$\alpha_{11} = -\frac{a_{22}}{2}\operatorname{Im}\left(\frac{\mu_1+\mu_2}{\mu_1\mu_2}\right), \tag{68}$$

$$\alpha_{22} = \frac{a_{11}}{2}\operatorname{Im}(\mu_1+\mu_2), \tag{69}$$

and

$$\alpha_{12} = -\frac{a_{22}}{2}\operatorname{Im}\left(\frac{1}{\mu_1\mu_2}\right) + \frac{a_{11}}{2}\operatorname{Im}(\mu_1\mu_2). \tag{70}$$

Regardless of how the auxiliary fields are defined, when Eq. (67) is applied to states 1, 2, and S, the following is produced:

$$\tilde{J}^{(1)} = \alpha_{11}K_{\text{I}}^{(1)2} + \alpha_{12}K_{\text{I}}^{(1)}K_{\text{II}}^{(1)} + \alpha_{22}K_{\text{II}}^{(1)2}, \tag{71}$$

$$\tilde{J}^{(2)} = \alpha_{11}K_{\text{I}}^{(2)2} + \alpha_{12}K_{\text{I}}^{(2)}K_{\text{II}}^{(2)} + \alpha_{22}K_{\text{II}}^{(2)2}, \tag{72}$$

and

$$\begin{aligned} \tilde{J}^{(S)} &= \alpha_{11}(K_{\text{I}}^{(1)} + K_{\text{I}}^{(2)})^2 + \alpha_{12}(K_{\text{I}}^{(1)} + K_{\text{I}}^{(2)}) \\ &\quad \times (K_{\text{II}}^{(1)} + K_{\text{II}}^{(2)}) + \alpha_{22}(K_{\text{II}}^{(1)} + K_{\text{II}}^{(2)})^2 \\ &= \alpha_{11}K_{\text{I}}^{(1)2} + \alpha_{12}K_{\text{I}}^{(1)}K_{\text{II}}^{(1)} + \alpha_{22}K_{\text{II}}^{(1)2} + \alpha_{11}K_{\text{I}}^{(2)2} \\ &\quad + \alpha_{12}K_{\text{I}}^{(2)}K_{\text{II}}^{(2)} + \alpha_{22}K_{\text{II}}^{(2)2} + 2\alpha_{11}K_{\text{I}}^{(1)}K_{\text{I}}^{(2)} \\ &\quad + \alpha_{12}(K_{\text{I}}^{(1)}K_{\text{II}}^{(2)} + K_{\text{I}}^{(2)}K_{\text{II}}^{(1)}) + 2\alpha_{22}K_{\text{II}}^{(1)}K_{\text{II}}^{(2)} \\ &= \tilde{J}^{(1)} + \tilde{J}^{(2)} + 2\alpha_{11}K_{\text{I}}^{(1)}K_{\text{I}}^{(2)} + \alpha_{12}(K_{\text{I}}^{(1)}K_{\text{II}}^{(2)} \\ &\quad + K_{\text{I}}^{(2)}K_{\text{II}}^{(1)}) + 2\alpha_{22}K_{\text{II}}^{(1)}K_{\text{II}}^{(2)}. \end{aligned} \tag{73}$$

By comparing Eqs. (59) and (73), the following can be obtained:

$$\tilde{M}^{(1,2)} = 2\alpha_{11}K_{\mathrm{I}}^{(1)}K_{\mathrm{I}}^{(2)} + \alpha_{12}(K_{\mathrm{I}}^{(1)}K_{\mathrm{II}}^{(2)} + K_{\mathrm{I}}^{(2)}K_{\mathrm{II}}^{(1)}) + 2\alpha_{22}K_{\mathrm{II}}^{(1)}K_{\mathrm{II}}^{(2)}. \tag{74}$$

If a similar procedure is followed and the intensity of the auxiliary state is judiciously chosen, as previously discussed, then the SIFs for non-homogeneous orthotropic materials can also be derived as

$$M^{(1,I)} = 2\alpha_{11}K_{\mathrm{I}}^{(1)} + \alpha_{12}K_{\mathrm{II}}^{(1)} \tag{75}$$

and

$$M^{(1,II)} = \alpha_{12}K_{\mathrm{I}}^{(1)} + 2\alpha_{22}K_{\mathrm{II}}^{(1)}, \tag{76}$$

where $M^{(1,\mathrm{I})}$ and $M^{(1,\mathrm{II})}$ are the mutual potential energy release rates for modes I and II, respectively and can be evaluated using Eq. (62). Eqs. (75) and (76) provide a system of linear algebraic equations that can be solved for SIFs $K_{\mathrm{I}}^{(1)}$ and $K_{\mathrm{II}}^{(1)}$ under various mixed-mode loading conditions. In general, a numerical method is required for calculating $M^{(1,\mathrm{I})}$ and $M^{(1,\mathrm{II})}$.

5. Numerical implementation

5.1. Finite element method

Consider a finite element discretization of a two-dimensional FGM cracked body involving N number of nodes. Let $\boldsymbol{z}_{\mathrm{I}}^{(1)} \in \mathbb{R}^2$ and $\boldsymbol{z}_{\mathrm{I}}^{(2)} \in \mathbb{R}^2$ be the actual and auxiliary displacement vectors, respectively, at the Ith node. If $\mathbf{d}^{(1)} = \{\boldsymbol{z}_{\mathrm{I}}^{(1)}\} \in \mathbb{R}^{2N}$; $I = 1, N$ and $\mathbf{d}^{(2)} = \{\boldsymbol{z}_{\mathrm{I}}^{(2)}\} \in \mathbb{R}^{2N}$; $I = 1, N$ represent global displacement vectors, the mutual potential energy release rate can be approximated by

$$\tilde{M}^{(1,2)} \cong \mathbf{d}^{(1)\mathrm{T}}\boldsymbol{K}'\mathbf{d}^{(2)} + \tfrac{1}{2}\mathbf{d}^{(2)\mathrm{T}}(\boldsymbol{K}' - \boldsymbol{K}'^{\mathrm{aux}})\mathbf{d}^{(2)}, \tag{77}$$

where $\boldsymbol{K}' = [\boldsymbol{k}'_{IJ}] \in \mathsf{L}(\mathbb{R}^{2N} \times \mathbb{R}^{2N})$; $I, J = 1, N$ and $\boldsymbol{K}'^{\mathrm{aux}} = [\boldsymbol{k}'^{\mathrm{aux}}_{IJ}] \in \mathsf{L}(\mathbb{R}^{2N} \times \mathbb{R}^{2N})$ are two global stiffness sensitivity matrices with $\boldsymbol{k}'_{IJ} \in \mathsf{L}(\mathbb{R}^2 \times \mathbb{R}^2)$ and $\boldsymbol{k}'^{\mathrm{aux}}_{IJ} \in \mathsf{L}(\mathbb{R}^2 \times \mathbb{R}^2)$ representing element-level (domain Ω_e) sensitivity matrices, given by

$$\boldsymbol{k}'_{IJ} = \int_{\Omega_e} (\boldsymbol{B}_{\mathrm{I}}^{\mathrm{T}}\boldsymbol{D}(\boldsymbol{x})\boldsymbol{B}'_J + \boldsymbol{B}_{\mathrm{I}}^{\mathrm{T}}\boldsymbol{D}(\boldsymbol{x})\boldsymbol{B}'_J - \boldsymbol{B}_{\mathrm{I}}^{\mathrm{T}}\boldsymbol{D}'(\boldsymbol{x})\boldsymbol{B}_J - \boldsymbol{B}_{\mathrm{I}}^{\mathrm{T}}\boldsymbol{D}(\boldsymbol{x})\boldsymbol{B}_J \mathrm{div}\boldsymbol{V})\,\mathrm{d}\Omega_e, \tag{78}$$

$$\boldsymbol{K}'^{\mathrm{aux}}_{IJ} = \int_{\Omega_e} (\boldsymbol{B}_{\mathrm{I}}^{\mathrm{T}}\boldsymbol{D}^{\mathrm{aux}}(\boldsymbol{x})\boldsymbol{B}'_J + \boldsymbol{B}_{\mathrm{I}}^{\mathrm{T}}\boldsymbol{D}^{\mathrm{aux}}(\boldsymbol{x})\boldsymbol{B}'_J - \boldsymbol{B}_{\mathrm{I}}^{\mathrm{T}}\boldsymbol{D}^{\mathrm{aux}}(\boldsymbol{x})\boldsymbol{B}_J \mathrm{div}\boldsymbol{V})\,\mathrm{d}\Omega_e. \tag{79}$$

In Eqs. (78) and (79),

$$\boldsymbol{B}_{\mathrm{I}}(\boldsymbol{x}) = \begin{bmatrix} \Phi_{I,1}(\boldsymbol{x}) & 0 \\ 0 & \Phi_{I,2}(\boldsymbol{x}) \\ \Phi_{I,2}(\boldsymbol{x}) & \Phi_{I,1}(\boldsymbol{x}) \end{bmatrix}, \tag{80}$$

$$\boldsymbol{B}'_{\mathrm{I}} = \begin{bmatrix} \Phi_{I,1}(\boldsymbol{x})V_{1,1}(\boldsymbol{x}) + \Phi_{I,2}(\boldsymbol{x})V_{2,1}(\boldsymbol{x}) & 0 \\ 0 & \Phi_{I,1}(\boldsymbol{x})V_{1,2}(\boldsymbol{x}) + \Phi_{I,2}(\boldsymbol{x})V_{2,2}(\boldsymbol{x}) \\ \Phi_{I,1}(\boldsymbol{x})V_{1,2}(\boldsymbol{x}) + \Phi_{I,2}(\boldsymbol{x})V_{2,2}(\boldsymbol{x}) & \Phi_{I,1}(\boldsymbol{x})V_{1,1}(\boldsymbol{x}) + \Phi_{I,2}(\boldsymbol{x})V_{2,1}(\boldsymbol{x}) \end{bmatrix}, \tag{81}$$

$$\boldsymbol{D}'(\boldsymbol{x}) = \frac{\partial \boldsymbol{D}(\boldsymbol{x})}{\partial x_1}V_1(\boldsymbol{x}) + \frac{\partial \boldsymbol{D}(\boldsymbol{x})}{\partial x_2}V_2(\boldsymbol{x}). \tag{82}$$

with $\Phi_{I,i}(\boldsymbol{x})$ serving as the partial derivatives of the shape function corresponding to the Ith node in the i direction. Eq. (77) can be viewed as a discrete analog of the continuum formulation in Eq. (62). The former involves simple matrix algebra and, as a result, provides a convenient means for calculating $\tilde{M}^{(1,2)}$.

5.2. Velocity field

Defining the velocity field is an important step in any continuum shape sensitivity analysis (Choi and Chang, 1994). For a fracture problem, the velocity field $\boldsymbol{V}(\boldsymbol{x})$ is defined with a compact support Ω_c, i.e., $\boldsymbol{V}(\boldsymbol{x})$, is non-*zero* when $\boldsymbol{x} \in \Omega_c$ and is *zero* when $\boldsymbol{x} \in \Omega - \Omega_c$, where $\Omega_c \subset \Omega$ is an appro-

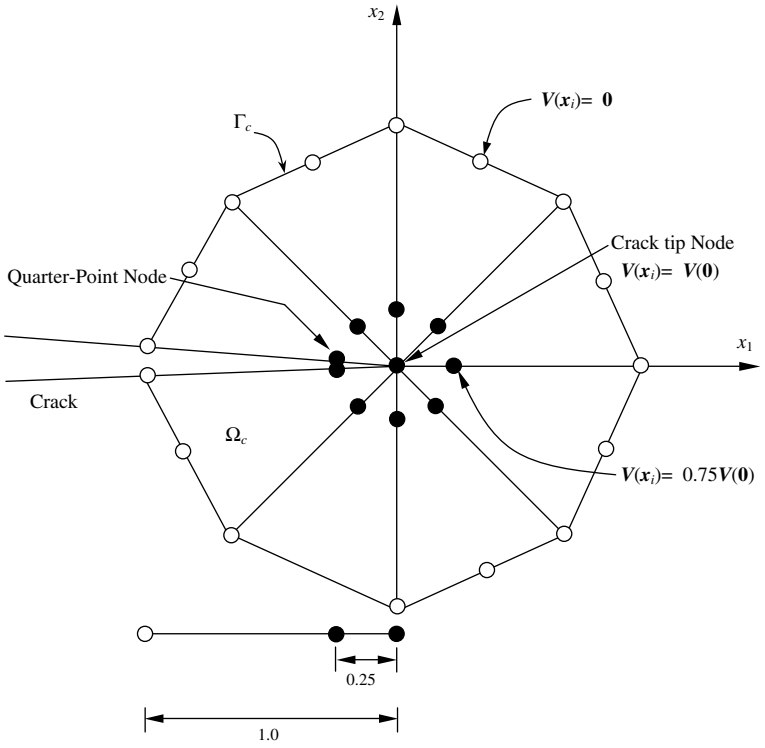

Fig. 3. Rosette of focused quarter-point 6-noded triangular elements near the crack tip.

priately small subdomain around the crack tip (see Fig. 1). Hence, the domain Ω in various integrals (see Eqs. (63)–(66)) can be replaced by the subdomain Ω_c. Specifically, consider a rosette of eight 6-noded quarter-point elements around a crack tip, as shown in Fig. 3. These quarter-point elements are standard finite elements commonly employed for fracture analysis of linear-elastic bodies. Assume that the size of these elements is small enough that the rosette can be defined as support Ω_c. Inside Ω_c, the velocity field satisfies the following conditions: (1) the crack tip is assigned a velocity of unit magnitude, i.e., $\boldsymbol{V}(\boldsymbol{0}) = (1/\sqrt{V_{1,\mathrm{tip}}^2 + V_{2,\mathrm{tip}}^2})\{V_{1,\mathrm{tip}}, V_{2,\mathrm{tip}}\}^{\mathrm{T}}$; (2) the velocity at a point on the boundary Γ_c of the rosette is *zero*; and (3) velocity at any point between boundary Γ_c and the crack tip varies linearly. For example, the velocity $\boldsymbol{V}(\boldsymbol{x}_i)$ at the ith node of the quarter-point elements in Fig. 3 can be defined as

$$\boldsymbol{V}(\boldsymbol{x}_i) = \begin{cases} \boldsymbol{0}, & \text{if } i \text{ is a node on the outer ring(open circles),} \\ 0.75\boldsymbol{V}(0), & \text{if } i \text{ is a quarter-point node (closed circles),} \\ \boldsymbol{V}(\boldsymbol{0}), & \text{if } i \text{ is the crack-tip node (closed circle).} \end{cases} \tag{83}$$

Since the velocity field is *zero* on and outside the outer boundary of the quarter point elements, Eq. (77) reduces to

$$\tilde{M}^{(1,2)} \cong \sum_{I,J=1}^{M} \boldsymbol{z}_{\mathrm{I}}^{(1)\mathrm{T}} \boldsymbol{K}'_{IJ} \boldsymbol{z}_J^{(2)} + \frac{1}{2} \sum_{I,J=1}^{M} \boldsymbol{z}_{\mathrm{I}}^{(2)\mathrm{T}} (\boldsymbol{K}'_{IJ} - \boldsymbol{K}'^{\mathrm{aux}}_{IJ}) \boldsymbol{z}_J^{(2)}, \tag{84}$$

where M is the total number of quarter-point and crack-tip nodes in a rosette of focused quarter-point elements near the crack tip, as shown by

the closed circles in Fig. 3. In other words, displacement response is only required at an M number of nodes. Since $M \ll N$, the effort in computing $\tilde{M}^{(1,2)}$ using Eq. (84) is trivial compared to that required for a complete stress analysis.

Compared with existing methods, the proposed method has several advantages: (1) the calculation of SIFs is simple and straightforward as it only requires multiplication of displacement vectors and stiffness sensitivity matrices; (2) since Ω_c is small and the velocity field outside Ω_c is zero, the method only requires displacement response in Ω_c, rendering it computationally efficient; (3) the accuracy of SIF estimates is not affected by a lack of smooth transition between mesh resolutions inside and outside Ω_c, as demonstrated by numerical results; and (4) the method is applicable to multiple interacting cracks even if crack tips are close to one other. Also, in contrast to existing methods, such as the J_k^*-integral method (Paulino, 2002), there is no need to perform integration along the crack face of the discontinuity (e.g., in calculating J_2^*). Hence, the proposed method is also simpler and more efficient than existing methods.

6. Numerical examples

In conjunction with the newly developed shape sensitivity method, standard FEM was applied to evaluate the SIFs of rectilinear cracks in two-dimensional orthotropic FGM structures. Both single-(mode I) and mixed-mode (modes I and II) conditions were considered and three examples are presented. For numerical integration purposes, a 2×2 Gauss quadrature rule was used for all examples. A plane stress condition and a crack-tip velocity $\{V_{1,\text{tip}}, V_{2,\text{tip}}\}^{\mathrm{T}} = \{10^{-5}a, 0\}^{\mathrm{T}}$ were also assumed. The results obtained in the current study were compared with the semi-analytical solutions by Oztuk and Erdogan (1997, 1999). For comparative purposes, the independent engineering constants, E_{11}, E_{22}, G_{12}, v_{12}, and v_{21} have been replaced by stiffness parameter E, a stiffness ratio δ^4, an average Poisson's ratio, and a shear parameter κ (Oztuk and Erdogan, 1997, 1999), which are defined as

$$\begin{aligned} &E = \sqrt{E_{11}E_{22}}, \quad \delta^4 = \frac{E_{11}}{E_{22}} = \frac{v_{12}}{v_{21}}, \\ &v = \sqrt{v_{12}v_{21}}, \quad \kappa = \frac{E}{2G_{12}} - v \end{aligned} \tag{85}$$

for plane stress, and

$$\begin{aligned} &E = \sqrt{\frac{E_{11}E_{22}}{(1-v_{13}v_{31})(1-v_{23}v_{32})}}, \\ &\delta^4 = \frac{E_{11}}{E_{22}}\frac{(1-v_{23}v_{32})}{(1-v_{13}v_{31})}, \\ &v = \sqrt{\frac{(v_{12}+v_{13}v_{32})(v_{21}+v_{23}v_{31})}{(1-v_{13}v_{31})(1-v_{23}v_{32})}}, \\ &\kappa = \frac{E}{2G_{12}} - v \end{aligned} \tag{86}$$

for plane strain.

6.1. Example 1: Plate with an interior crack parallel to material gradation under Mode-I

Consider an orthotropic square plate of dimensions $2L = 2W = 20$ *units* ($L/W = 1$) with a central crack of length $2a = 2.0$ *units*, as shown in Fig. 4(a). Both crack-face pressure loading, and fixed grip loading (under a constant strain) were considered. The crack runs parallel to the material gradation, and the following material property data were employed for FEM analysis: $E_{11}(x_1) = E_{11}^0 e^{\beta x_1}$, $E_{22}(x_1) = E_{22}^0 e^{\beta x_1}$, $G_{12}(x_1) = G_{12}^0 e^{\beta x_1}$, where the average modulus of elasticity $E(x_1) = E_0 e^{\beta a\left(\frac{x_1}{a}\right)}$, with $E^0 = \sqrt{E_{11}^0 E_{22}^0}$. The non-homogeneity parameter βa is varied from 0.0 to 1.0. Two different values of the shear parameter $\kappa = -0.25$ and 5.0 were employed. The average Poisson's ratio v is varied between 0.1 and 0.9. The stiffness ratio $\delta^4 = 0.25$ was used in FEM analysis.

For crack-face pressure loading, the applied load corresponds to $\sigma_{22}(-1 \leqslant x_1 \leqslant 1, \pm 0) = \pm\sigma_0 = \pm 1.0$ along the top and bottom crack faces; and for fixed grip loading, the applied load results in a uniform strain $\varepsilon(x_1, x_2) = \varepsilon_0$ for a corresponding uncracked plate. The displacement boundary condition is prescribed, such that $u_1 = u_2 = 0$ for the node in the middle of the left edge, and $u_2 = 0$ for the node in the middle of the right edge. FEM discretization involves 2808 nodes, 864

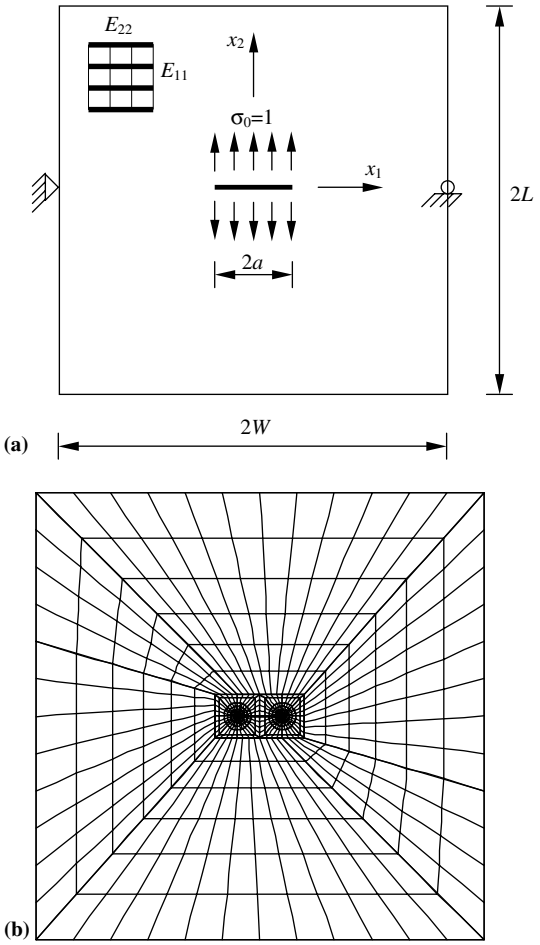

Fig. 4. Plate with an interior crack parallel to material gradation under mode-I: (a) geometry and loads; (b) FEM discretization (2808 nodes, 864 8-noded quadrilateral elements, and 32 focused quarter-point 6-noded triangular elements).

8-noded quadrilateral elements, and 32 focused quarter-point 6-noded triangular elements in the vicinity of each crack tip, as shown in Fig. 4(b).

Oztuk and Erdogan (1997) investigated an infinite plate with the same configuration. Obviously, an FEM model cannot represent the infinite domains addressed in their analysis, but as long as the ratios a/W and a/L are kept relatively small (e.g., $a/W = a/L \leqslant 1/10$), the approximation is acceptable. Tables 1 and 2 provide a comparison between predicted normalized stress intensity factors $K_I(a)/\sigma_0\sqrt{\pi a}$ and $K_I(-a)/\sigma_0\sqrt{\pi a}$ at both crack tips for several values of the non-homogeneous parameter βa, obtained by using the proposed method, and those of Oztuk and Erdogan (1997). In Table 1 the shear parameter is $\kappa = -0.25$, whereas in Table 2 the shear parameter is $\kappa = 5.0$. Numerical results from the proposed method show that the effect of κ on normalized stress intensity factors is less significant than that of βa. In addition, the stress intensity factor on the stiffer side of the medium is always greater than that on the less stiff side. Tables 3 and 4 provide a comparison between predicted normalized stress intensity factors $K_I(a)/\sigma_0\sqrt{\pi a}$ and $K_I(-a)/\sigma_0\sqrt{\pi a}$ under uniform crack face pressure loading at both crack tips for several values of Poisson's ratio ν, obtained using the proposed method, and those of Oztuk and Erdogan (1997) for shear parameter $\kappa = 0.5$. In Table 3 the non-homogeneous

Table 1
Normalized stress intensity factors for an orthotropic plate under uniform crack face pressure loading ($\kappa = -0.25$)

βa	Proposed method		Oztuk and Erdogan (1997)	
	$\frac{K_I(a)}{\sigma_0\sqrt{\pi a}}$	$\frac{K_I(-a)}{\sigma_0\sqrt{\pi a}}$	$\frac{K_I(a)}{\sigma_0\sqrt{\pi a}}$	$\frac{K_I(-a)}{\sigma_0\sqrt{\pi a}}$
0.0	1.0108	1.0108	1.0	1.0
0.01	1.0135	1.0081	1.0025	0.9975
0.1	1.0377	0.9837	1.0246	0.9747
0.25	1.0764	0.9426	1.0604	0.9364
0.50	1.1292	0.8709	1.1177	0.8740
0.75	1.1703	0.8023	1.1720	0.8154
1.00	1.2139	0.7443	1.2235	0.7616
1.50	1.3062	0.6506	1.3184	0.6701
2.00	1.3916	0.5773	1.4043	0.5979

Table 2
Normalized stress intensity factors for an orthotropic plate under uniform crack face pressure loading ($\kappa = 5.0$)

βa	Proposed method		Oztuk and Erdogan (1997)	
	$\frac{K_I(a)}{\sigma_0\sqrt{\pi a}}$	$\frac{K_I(-a)}{\sigma_0\sqrt{\pi a}}$	$\frac{K_I(a)}{\sigma_0\sqrt{\pi a}}$	$\frac{K_I(-a)}{\sigma_0\sqrt{\pi a}}$
0.0	1.0338	1.0338	1.0	1.0
0.01	1.0365	1.0310	1.0025	0.9975
0.1	1.0611	1.0062	1.0231	0.9733
0.25	1.0994	0.9628	1.0531	0.9306
0.50	1.1458	0.8840	1.0946	0.8594
0.75	1.1740	0.8066	1.1281	0.7932
1.00	1.1921	0.7375	1.1556	0.7339
1.50	1.2142	0.6277	1.1979	0.6367
2.00	1.2310	0.5493	1.2290	0.5636

Table 3
The effect of Poisson's ratio on the normalized stress intensity factors for an orthotropic plate under uniform crack face pressure loading ($\beta a = 0.5$, $\kappa = 0.5$)

ν	Proposed method		Oztuk and Erdogan (1997)	
	$\frac{K_I(a)}{\sigma_0\sqrt{\pi a}}$	$\frac{K_I(-a)}{\sigma_0\sqrt{\pi a}}$	$\frac{K_I(a)}{\sigma_0\sqrt{\pi a}}$	$\frac{K_I(-a)}{\sigma_0\sqrt{\pi a}}$
0.1	1.1116	0.8599	1.0958	0.8602
0.2	1.1157	0.8627	1.1007	0.8633
0.3	1.1196	0.8655	1.1053	0.8661
0.4	1.1235	0.8682	1.1096	0.8689
0.5	1.1273	0.8709	1.1137	0.8715
0.7	1.1349	0.8763	1.1215	0.8764
0.9	1.1433	0.8824	1.1287	0.8809

Table 4
The effect of Poisson's ratio on the normalized stress intensity factors for an orthotropic plate under uniform crack face pressure loading ($\beta a = 1.0$, $\kappa = 0.5$)

ν	Proposed method		Oztuk and Erdogan (1997)	
	$\frac{K_I(a)}{\sigma_0\sqrt{\pi a}}$	$\frac{K_I(-a)}{\sigma_0\sqrt{\pi a}}$	$\frac{K_I(a)}{\sigma_0\sqrt{\pi a}}$	$\frac{K_I(-a)}{\sigma_0\sqrt{\pi a}}$
0.1	1.1509	0.7185	1.1594	0.7354
0.2	1.1661	0.7250	1.1739	0.7413
0.3	1.1806	0.7312	1.1874	0.7468
0.4	1.1943	0.7371	1.2001	0.7520
0.5	1.2073	0.7427	1.2121	0.7569
0.7	1.2318	0.7535	1.2343	0.7661
0.9	1.2556	0.7644	1.2546	0.7746

Table 5
The effect of Poisson's ratio on the normalized stress intensity factors for an orthotropic plate under fixed-grip loading ε_0 ($\overline{E}_0 = E_0/\delta^4$, $\beta a = 0.5$, $\kappa = 0.5$)

ν	Proposed method		Oztuk and Erdogan (1997)	
	$\frac{K_I(a)}{\varepsilon_0\overline{E}_0\sqrt{\pi a}}$	$\frac{K_I(-a)}{\varepsilon_0\overline{E}_0\sqrt{\pi a}}$	$\frac{K_I(a)}{\varepsilon_0\overline{E}_0\sqrt{\pi a}}$	$\frac{K_I(-a)}{\varepsilon_0\overline{E}_0\sqrt{\pi a}}$
0.1	1.4224	0.6650	1.4183	0.6647
0.2	1.4255	0.6669	1.4233	0.6676
0.3	1.4285	0.6687	1.4280	0.6704
0.4	1.4314	0.6705	1.4325	0.6730
0.5	1.4343	0.6723	1.4368	0.6755
0.7	1.4400	0.6757	1.4449	0.6802
0.9	1.4471	0.6798	1.4524	0.6846

parameter is $\beta a = 0.5$, while in Table 4 the non-homogeneous parameter is $\beta a = 1$. Tables 5 and 6 provide a similar comparison between predicted

Table 6
The effect of Poisson's ratio on the normalized stress intensity factors for an orthotropic plate under fixed-grip loading ε_0 ($\overline{E}_0 = E_0/\delta^4$, $\beta a = 1.0$, κ=0.5)

ν	Proposed method		Oztuk and Erdogan (1997)	
	$\frac{K_I(a)}{\varepsilon_0\overline{E}_0\sqrt{\pi a}}$	$\frac{K_I(-a)}{\varepsilon_0\overline{E}_0\sqrt{\pi a}}$	$\frac{K_I(a)}{\varepsilon_0\overline{E}_0\sqrt{\pi a}}$	$\frac{K_I(-a)}{\varepsilon_0\overline{E}_0\sqrt{\pi a}}$
0.1	2.0673	0.4371	1.9991	0.4265
0.2	2.0716	0.4395	2.0151	0.4319
0.3	2.0762	0.4419	2.0301	0.4368
0.4	2.0812	0.4444	2.0442	0.4415
0.5	2.0864	0.4469	2.0576	0.4459
0.7	2.0976	0.4520	2.0826	0.4541
0.9	2.1116	0.4576	2.1056	0.4616

normalized stress intensity factors $K_I(a)/\varepsilon_0\overline{E}_0\sqrt{\pi a}$ and $K_I(-a)/\varepsilon_0\overline{E}_0\sqrt{\pi a}$ under fixed-grip loading. These results shows that Poisson's ratio has a negligible effect on the SIFs for a mode I crack problem. The agreement between present results using the proposed method and Oztuk and Erdogan's (1997) analytical solution is excellent.

6.2. Example 2: Plate with an interior crack perpendicular to material gradation (mixed mode)

Consider an orthotropic square plate of dimensions $2L = 2W = 20$ *units* ($L/W = 1$) with a central crack of length $2a = 2.0$ *units*, as shown in Fig. 5. Except for material properties and loading condi-

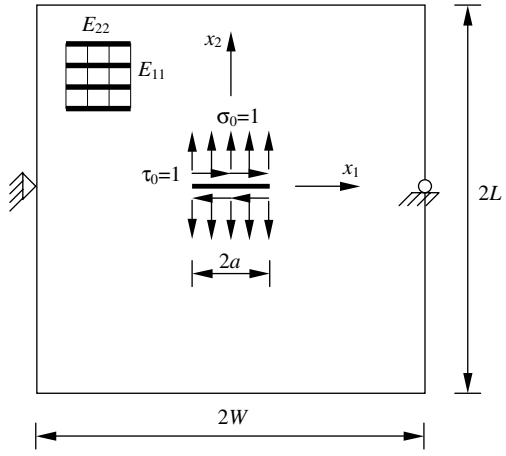

Fig. 5. Plate with an interior crack perpendicular to material gradation: geometry and loads.

tions, all other conditions including FEM discretization were the same as in Example 1. However, the crack is perpendicular to the material gradation. In Example 2, both crack-face pressure loading and crack-face shear loading were considered separately. The following material property data were employed for FEM analysis: $E_{11}(x_2) = E^0_{11}e^{\beta x_2}$, $E_{22}(x_2) = E^0_{22}e^{\beta x_2}$, $G_{12}(x_2) = G^0_{12}e^{\beta x_2}$, where the average modulus of elasticity is $E(x_2) = E^0e^{\beta a(\frac{x_2}{a})}$, with $E^0 = \sqrt{E^0_{11}E^0_{22}}$. The non-homogeneity parameter βa is varied from 0.0 to 2.0. Two different values of the shear parameter $\kappa = 0.5$ and 5.0 and two different stiffness ratios $\delta^4 = 0.25$, and 10 were employed in the FEM analysis. Three different values of the average Poisson's ratio $\nu = 0.15$, 0.30, and 0.45 were used in computations.

For crack-face pressure loading the applied load corresponds to $\sigma_{22}(-1 \leqslant x_1 \leqslant 1, \pm 0) = \pm\sigma_0 = \pm 1.0$ and for crack-face shear loading the applied load corresponds to $\sigma_{12}\ (-1 \leqslant x_1 \leqslant 1, \pm 0) = \pm\tau_0 = \pm 1.0$ along the top and bottom crack faces.

The effect of the non-homogeneity parameter βa and the average Poisson's ratio ν on normalized stress intensity factors for both crack-face pressure loading and crack-face shear loading were studied. The results obtained by using the proposed method are compared with those reported by Oztuk and Erdogan (1999), who investigated an infinite plate with the same configuration. Tables 7 and 8 provide a comparison between predicted normalized stress intensity factors $K_I(a)/\sigma_0\sqrt{\pi a}$ and $K_I(-a)/\sigma_0\sqrt{\pi a}$ under uniform crack-face pressure loading and uniform crack-face shear loading,

Table 7
The effect of the non-homogeneity parameter on the normalized stress intensity factors for an orthotropic plate under uniform crack face pressure loading ($\delta^4 = 0.25$, $\nu = 0.3$, κ=0.5)

βa	Proposed method		Oztuk and Erdogan (1999)	
	$\frac{K_I(a)}{\sigma_0\sqrt{\pi a}}$	$\frac{K_{II}(a)}{\sigma_0\sqrt{\pi a}}$	$\frac{K_I(a)}{\sigma_0\sqrt{\pi a}}$	$\frac{K_{II}(a)}{\sigma_0\sqrt{\pi a}}$
0.0	1.0091	0.0009	1.0	0.0
0.1	1.0158	0.0262	1.0115	0.0250
0.25	1.0451	0.0643	1.0489	0.0627
0.50	1.1279	0.1288	1.1351	0.1263
1.00	1.3468	0.2632	1.3494	0.2587
2.00	1.8673	0.5607	1.8580	0.5529

Table 8
The effect of the non-homogeneity parameter on the normalized stress intensity factors for an orthotropic plate under uniform crack face shear loading ($\delta^4 = 0.25$, $\nu = 0.3$, κ=0.5)

βa	Proposed method		Oztuk and Erdogan (1999)	
	$\frac{K_I(a)}{\tau_0\sqrt{\pi a}}$	$\frac{K_{II}(a)}{\tau_0\sqrt{\pi a}}$	$\frac{K_I(a)}{\tau_0\sqrt{\pi a}}$	$\frac{K_{II}(a)}{\tau_0\sqrt{\pi a}}$
0.0	0.0108	0.9924	0.0	1.0
0.1	−0.0389	0.9914	−0.0494	0.9989
0.25	−0.1098	0.9861	−0.1191	0.9968
0.50	−0.2130	0.9799	−0.2217	0.9965
1.00	−0.3781	0.9899	−0.3862	1.0071
2.00	−0.6178	1.0358	−0.5725	1.0499

respectively, obtained by using the proposed method, and those of Oztuk and Erdogan (1999) for various values of non-homogeneity parameter βa, and $\delta^4 = 0.25$; $\nu = 0.3$; and $\kappa = 0.5$. Tables 9 and 10 provide a comparison between predicted normalized stress intensity factors under uniform crack face pressure loading for $\delta^4 = 0.25$, and $\delta^4 = 10$ respectively, obtained by the proposed method, and those of Oztuk and Erdogan (1999) for $\nu = 0.15$, 0.3, and 0.45 and $\beta a = 0.5$, and 1.0. Tables 11 and 12 provide a similar comparison for an orthotropic plate under uniform crack face shear loading. The agreement between the results of the proposed method and Oztuk and Erdogan's (1999) analytical solution is excellent.

6.3. Example 3: Four-point bending specimen under mixed-mode loading

Gu and Asaro (1997) investigated the effect of material orthotropy on mixed-mode SIFs in FGMs by considering a four-point bending specimen with exponentially varying Young's moduli, shear modulus, and Poisson's ratio. Fig. 6(a) shows the geometry and boundary conditions of the four-point bending specimen. Due to symmetric geometry and loading with respect to the crack, only a half model of the beam was analyzed, as shown in Fig. 6(b). Fig. 6(c) shows details of FEM mesh discretization for the half beam model involving 1357 nodes, 396 8-noded quadrilateral elements, and 32 focused quarter-point 6-noded triangular elements in the vicinity of the crack tip. Point loads of magnitude P are applied at

Table 9
The effect of Poisson's ratio on the normalized stress intensity factors for an orthotropic plate under uniform crack face pressure loading ($\kappa = 5.0$)

βa	$\delta^4 = 0.25$	Proposed method			Oztuk and Erdogan (1999)		
	v	0.15	0.30	0.45	0.15	0.30	0.45
0.5	$K_I(a)/\sigma_0\sqrt{\pi a}$	1.2463	1.2545	1.2625	1.2516	1.2596	1.2674
	$K_{II}(a)/\sigma_0\sqrt{\pi a}$	0.1264	0.1270	0.1275	0.1259	0.1259	0.1259
1.0	$K_I(a)/\sigma_0\sqrt{\pi a}$	1.5596	1.5750	1.5901	1.5589	1.5739	1.5884
	$K_{II}(a)/\sigma_0\sqrt{\pi a}$	0.2580	0.2588	0.2595	0.2555	0.2557	0.2558

Table 10
The effect of Poisson's ratio on the normalized stress intensity factors for an orthotropic plate under uniform crack face pressure loading ($\kappa = 5.0$)

βa	$\delta^4 = 10$	Proposed method			Oztuk and Erdogan (1999)		
	v	0.15	0.30	0.45	0.15	0.30	0.45
0.5	$K_I(a)/\sigma_0\sqrt{\pi a}$	1.0599	1.0605	1.0610	1.0748	1.0776	1.0804
	$K_{II}(a)/\sigma_0\sqrt{\pi a}$	0.1235	0.1238	0.1241	0.1252	0.1252	0.1251
1.0	$K_I(a)/\sigma_0\sqrt{\pi a}$	1.1746	1.1757	1.1769	1.1892	1.1955	1.2017
	$K_{II}(a)/\sigma_0\sqrt{\pi a}$	0.2500	0.2503	0.2506	0.2511	0.2512	0.2512

Table 11
The effect of Poisson's ratio on the normalized stress intensity factors for an orthotropic plate under uniform crack face shear loading ($\kappa = 5.0$)

βa	$\delta^4 = 0.25$	Proposed method			Oztuk and Erdogan (1999)		
	v	0.15	0.30	0.45	0.15	0.30	0.45
0.5	$K_I(a)/\tau_0\sqrt{\pi a}$	−0.1921	−0.1912	−0.1903	−0.1980	−0.1971	−0.1963
	$K_{II}(a)/\tau_0\sqrt{\pi a}$	0.9600	0.9614	0.9627	0.9898	0.9915	0.9931
1.0	$K_I(a)/\tau_0\sqrt{\pi a}$	−0.3177	−0.3159	−0.3141	−0.3203	−0.3186	−0.3169
	$K_{II}(a)/\tau_0\sqrt{\pi a}$	0.9556	0.9587	0.9617	0.9888	0.9921	0.9953

Table 12
The effect of Poisson's ratio on the normalized stress intensity factors for an orthotropic plate under uniform crack face shear loading ($\kappa = 5.0$)

βa	$\delta^4 = 10$	Proposed method			Oztuk and Erdogan (1999)		
	v	0.15	0.30	0.45	0.15	0.30	0.45
0.5	$K_I(a)/\tau_0\sqrt{\pi a}$	−0.0328	−0.0328	−0.0328	−0.0366	−0.0365	−0.0365
	$K_{II}(a)/\tau_0\sqrt{\pi a}$	0.9419	0.9419	0.9419	0.9956	0.9961	0.9965
1.0	$K_I(a)/\tau_0\sqrt{\pi a}$	−0.0625	−0.0625	−0.0625	−0.0660	−0.0657	−0.0654
	$K_{II}(a)/\tau_0\sqrt{\pi a}$	0.9355	0.9357	0.9358	0.9913	0.9925	0.9938

the nodes $(x_1, x_2) = (10, -1.0)$ and $(x_1, x_2) = (11, 1.0)$. Displacement boundary conditions are prescribed such that $(u_1, u_2) = (0, 0)$ for the node at $(x_1, x_2) = (0, -1.0)$, and $u_1 = 0$ for the node at $(x_1, x_2) = (0, 0)$. Young's moduli, the shear modulus, and Poisson's ratio are exponential functions

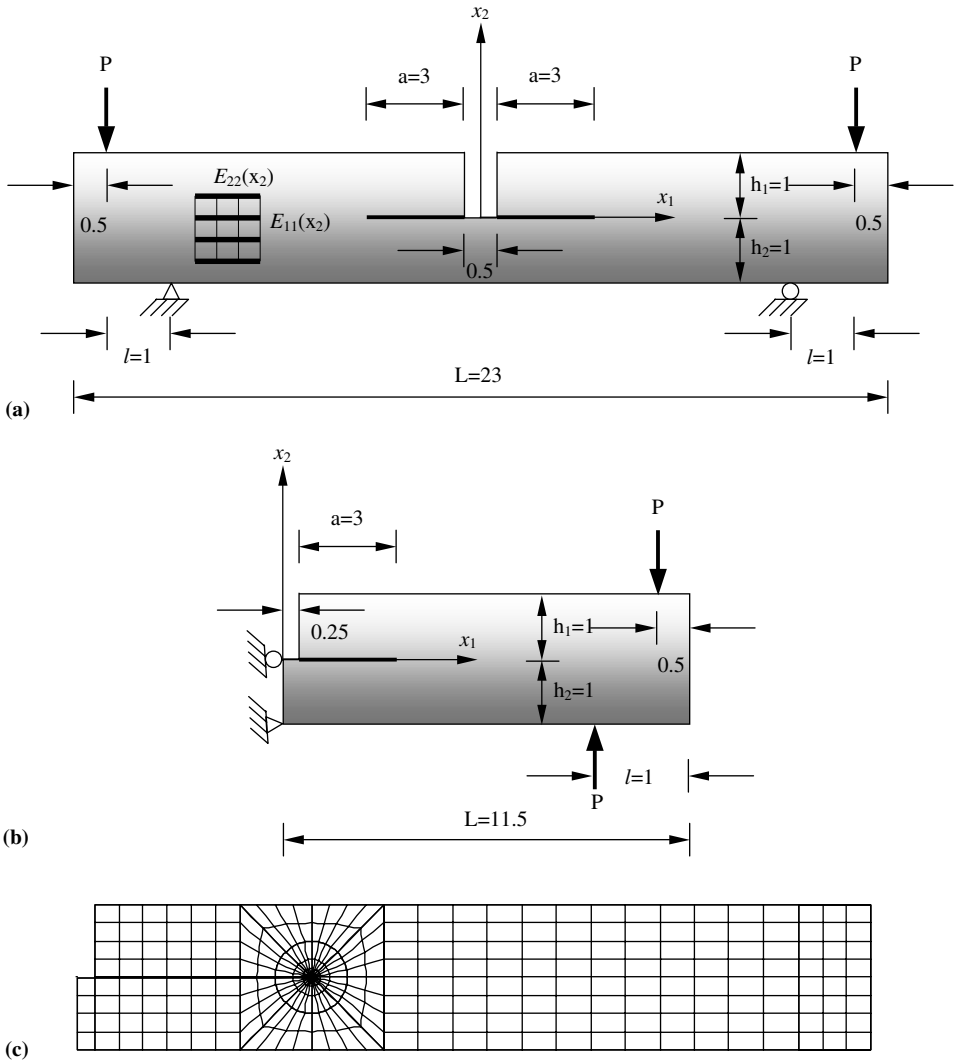

Fig. 6. Four-point bend specimen under mixed mode loading: (a) Geometry and loads; (b) Half model; (c) FEM discretization (1357 nodes, 396 8-noded quadrilateral elements, and 32 focused quarter-point 6-noded triangular elements).

of x_2 given by: $E_{11}(x_2) = E^0_{11}e^{\beta x_2}$, $E_{22}(x_2) = E^0_{22}e^{\beta x_2}$, $v_{12}(x_2) = v^0_{12}(1+\varepsilon x_2)e^{\beta x_2}$, $v_{21}(x_2) = v^0_{21}\ (1+\varepsilon x_2) \times e^{\beta x_2}$, and $G_{12}(x_2) = E_{22}(x_2)/[2(\sqrt{\lambda}+v_{21}\ (x_2))]$,where $\lambda = E_{22}(x_2)/E_{11}(x_2)$. Notice that $\lambda = 1/\delta^4$, as explained in Eqs. (85) and (86). The following data were used for the FEM analysis: $a = 3.0$, $h_1/h_2 = 1.0$, $\varepsilon = -0.9$, and $P = 1.0$.

Fig. 7(a) and (b) provide a comparison of the SIF $|K|h_1^{3/2}/Pl$ with $|K| = \sqrt{K_I^2 + K_{II}^2}$, and the phase angle $\psi = \tan^{-1}(K_{II}/K_I)$, respectively, obtained by the proposed continuum shape sensitivity method with those values reported by Gu and Asaro (1997). There is quite good agreement between the two solutions, although Gu and Asaro (1997) did not provide geometry data. Notice that as βh_1 increases, both the SIF and the phase angle ψ increase, and the material orthotropy (measured by $\lambda = E_{22}/E_{11}$) shows significant influence on the results. Moreover, for a fixed βh_1, as λ increases

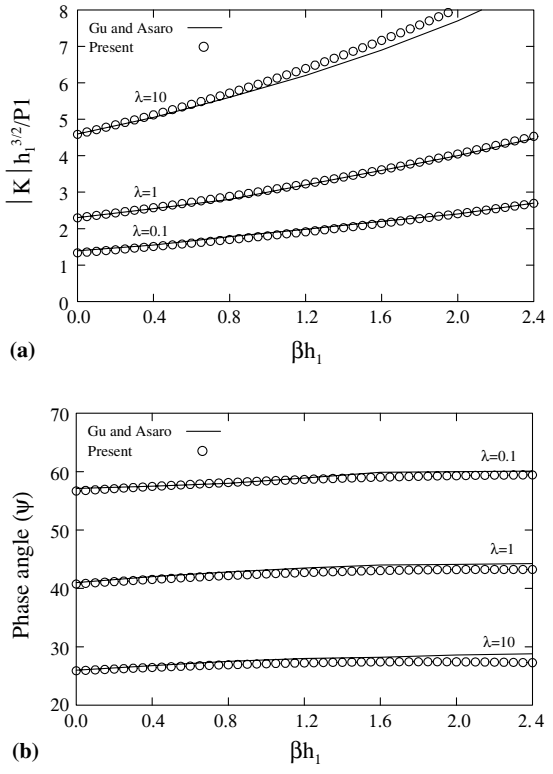

Fig. 7. Four-point bend specimen under mixed mode loading: (a) normalized mixed-mode SIFs $|K|h_1^{3/2}/Pl$; (b) phase angle $\psi = \tan^{-1}(K_{II}/K_I)$.

the SIF increases; however, the phase angle decreases.

7. Summary and conclusions

A new continuum shape sensitivity method was developed for calculating mixed-mode stress-intensity factors for a stationary crack in two-dimensional, linear-elastic, isotropic FGMs having an arbitrary geometry. The method involves the material derivative concept taken from continuum mechanics, the mutual potential energy release rate, and direct differentiation. Since the governing variational equation is differentiated prior to discretization, the resulting sensitivity equations are independent of approximate numerical techniques, such as the finite element method, boundary element method, mesh-free method, or others. The discrete form of the mutual potential energy release rate is simple and easy to calculate, as it only requires multiplication of displacement vectors and stiffness sensitivity matrices. By judiciously selecting the velocity field, the method only requires displacement response in a subdomain close to the crack tip, thus rendering it computationally efficient. Three numerical examples, including both mode-I and mixed-mode problems, are presented to evaluate the accuracy of fracture parameters calculated using the proposed method. Comparisons have been made between the stress-intensity factors predicted by the proposed method and available reference solutions in the literature, generated either analytically or numerically using various other fracture integrals or analyses. An excellent agreement is obtained between the results of the proposed method and previously obtained solutions. Therefore, shape sensitivity analysis provides an attractive alternative for the fracture analysis of cracks in homogeneous and non-homogeneous orthotropic materials.

Acknowledgment

The authors would like to acknowledge the financial support of the US National Science Foundation (NSF) under Award Nos. CMS-9733058 and CMS-04094632.

References

Bonnet, M., 2001. Boundary element based formulations for crack shape sensitivity analysis. Engineering Analysis with Boundary Elements 25, 347–362.

Céa, J., 1981. Problems of shape optimal design. In: Haug, E.J., Céa, J. (Eds.), Optimization of Distributed Parameters Structures. Sijthoff and Noordhoff, Alphen a/d Rijn.

Chen, G., Rahman, S., Park, Y.H., 2001a. Shape sensitivity and reliability analyses of linear-elastic cracked structures. International Journal of Fracture 112 (3), 223–246.

Chen, G., Rahman, S., Park, Y.H., 2001b. Shape sensitivity analysis in mixed-mode fracture mechanics. Computational Mechanics 27 (4), 282–291.

Chen, G., Rahman, S., Park, Y.H., 2002. Shape sensitivity analysis of linear-elastic cracked structures. ASME Journal of Pressure Vessel Technology 124 (4), 476–482.

Choi, K.K., Chang, K.H., 1994. A study of design velocity field computation for shape optimal design. Finite Elements in Analysis and Design 15, 317–341.

Erdogan, F., 1995. Fracture mechanics of functionally graded materials. Composites Engineering 5 (7), 753–770.

Feijóo, R.A., Padra, C., Saliba, R., Taroco, E., Vénere, M.J., 2000. Shape sensitivity analysis for energy release rate evaluation and its application to the study of three-dimensional cracked bodies. Computer Methods in Applied Mechanics and Engineering 188, 649–664.

Fuenmayor, J., Dominguez, J., Giner, E., Oliver, J.L., 1997. Calculation of the stress intensity factor and estimation of its error by a shape sensitivity analysis. Fatigue and Fracture in Engineering Materials and Structures 20 (5), 813–828.

Giner, E., Fuenmayor, F.J., Besa, A.J., Tur, M., 2002. An implementation of the stiffness derivative method as a discrete analytical sensitivity analysis and its application to mixed mode in LEFM. Engineering Fracture Mechanics 69 (18), 2051–2071.

Gu, P., Asaro, R.J., 1997. Cracks in functionally graded materials. International Journal of Solids and Structures 34, 1–17.

Gurtin, M.E., 1981. An Introduction to Continuum Mechanics. Academic Press, New York, NY.

Haug, E.J., Choi, K.K., Komkov, V., 1986. Design Sensitivity Analysis of Structural Systems. Academic Press, New York, NY.

Hwang, C.G., Wawrzynek, P.A., Tayebi, A.K., Ingraffea, A.R., 1998. On the virtual crack extension method for calculation of the rates of energy release rate. Engineering Fracture Mechanics 59 (4), 521–542.

Kaysser, W.A., Ilschner, B., 1995. FGM research activities in Europe. M.R.S. Bulletin 20 (1), 22–26.

Kim, J.H., Paulino, G.H., 2002. Mixed-mode fracture of orthotropic functionally graded materials using finite elements and the modified crack closure method. Engineering Fracture Mechanics 69, 1557–1586.

Lee, T.W., Grosse, I.R., 1993. Energy release rate by a shape design sensitivity approach. Engineering Fracture Mechanics 44 (5), 807–819.

Lekhnitskii, S.G., Tsai, S.W., Cheron, T., 1986. Anisotropic Plates. Gorden and Breach Science Publishers, New York.

Oztuk, M., Erdogan, F., 1997. Mode I crack problem in an inhomogeneous orthotropic medium. International Journal of Engineering Science 35 (9), 869–883.

Oztuk, M., Erdogan, F., 1999. The mixed mode crack problem in an inhomogeneous orthotropic medium. International Journal of Fracture 98, 243–261.

Paulino, G.H., 2002. Fracture of functionally graded materials. Engineering Fracture Mechanics 69 (14-16), 1519–1520.

Rao, B.N., Rahman, S., 2003a. Meshfree analysis of cracks in isotropic functionally graded materials. Engineering Fracture Mechanics 70, 1–27.

Rao, B.N., Rahman, S., 2003b. An interaction integral method for analysis of cracks in orthotropic functionally graded materials. Computational Mechanics 32 (1–2), 40–51.

Rao, B.N., Rahman, S., submitted for publication. A continuum shape sensitivity method for fracture analysis of isotropic functionally graded materials. Computational Mechanics.

Sampath, S., Herman, H., Shimoda, N., Saito, T., 1995. Thermal spray processing of FGMs. M.R.S. Bulletin 20 (1), 27–31.

Shih, G.C., Paris, P.C., Irwin, G.R., 1965. On cracks in rectilinearly anisotropic bodies. International Journal of Fracture 1, 189–203.

Suresh, S., Mortensen, A., 1998. Fundamentals of Functionally Graded Materials. IOM Communications Ltd., London.

Taroco, E., 2000. Shape sensitivity analysis in linear elastic fracture mechanics. Computer Methods in Applied Mechanics and Engineering 188, 697–712.